FINAL REPORT

STUDY, SELECTION, AND PREPARATION OF SOLID CATIONIC CONDUCTORS

by

W. L. Roth, S. P. Mitoff, and R. N. King

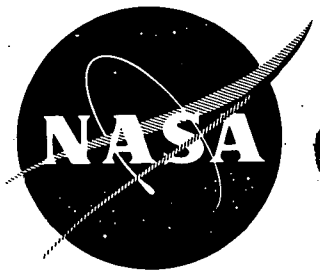

GENERAL ELECTRIC COMPANY
CORPORATE RESEARCH AND DEVELOPMENT
Physical Chemistry Laboratory
P.O. Box 8, Schenectady, New York 12301

prepared for

NATIONAL AERONAUTICS AND SPACE ADMINISTRATION

September 1972

CONTRACT NAS3-15692

NASA Lewis Research Center
Cleveland, Ohio

Albert Antoine, Project Manager

1. Report No.	2. Government Accession No.	3. Recipient's Catalog No.
CR-120964		

4. Title and Subtitle	5. Report Date
STUDY, SELECTION, AND PREPARATION OF SOLID CATIONIC CONDUCTORS	September 1972
	6. Performing Organization Code

7. Author(s)	8. Performing Organization Report No.
W. L. Roth, S. P. Mitoff, and R. N. King	SRD-72-116
	10. Work Unit No.

9. Performing Organization Name and Address	11. Contract or Grant No.
General Electric Company P.O. Box 8 Schenectady, New York 12301	NAS3-15692
	13. Type of Report and Period Covered Final Report July 1, 1971 - June 30, 1972

12. Sponsoring Agency Name and Address	14. Sponsoring Agency Code
National Aeronautics and Space Administration Washington, D. C. 20546	

15. Supplementary Notes Project Managers: Fritz G. Will, General Electric Corporate Research and Development, P. O. Box 8, Schenectady, N. Y. 12301
Albert C. Antoine, Energy Conversion and Material Science Division, NASA Lewis Research Center, Cleveland, Ohio.

16. Abstract

Crystal chemical principles and transport theory have been used to predict structures and specific compounds which might find application as solid electrolytes in rechargeable high energy and high power density batteries operating at temperatures less than 200°C. More than twenty compounds were synthesized or obtained and screened by nuclear magnetic resonance and conductivity. Many were densified by sintering or hot pressing. Encouraging results have been obtained for nine of these materials but none have yet been good ionic conductors at low temperature.

17. Key Words (Suggested by Author(s))	18. Distribution Statement
Ionic conductors Solid electrolytes Batteries Nuclear Magnetic Resonance Transport numbers	Unclassified, Unlimited

19. Security Classif. (of this report)	20. Security Classif. (of this page)	21. No. of Pages	22. Price*
Unclassified	Unclassified	56	

* For sale by the National Technical Information Service, Springfield, Virginia 22151

FOREWORD

The nuclear magnetic resonance spectra described herein were measured by I. Chung, D. Kline, and H. Story in the Physics Laboratories of the State University of New York at Albany.

TABLE OF CONTENTS

LIST OF ILLUSTRATIONS

List of Illustrations (continued)

I. SUMMARY

A proposal entitled "Study, Selection, and Preparation of Solid Cationic Conductors" was submitted to NASA in May 1971, in response to RFP No. 416187. It described a research program aimed at the identification and preparation of materials for use as non-porous solid ionic conductors in rechargeable high-energy and power density battery systems operating at temperatures less than 200°C. The proposal also presented a summary of the status of solid electrolytes. The only materials capable of meeting the required objectives that had been identified at that time were members of the beta-alumina family. The research proposal outlined theoretical and crystal chemical criteria for the selection of potential solid ionic conductors and described experimental procedures for screening and evaluating the ion transport properties of a wide range of new materials with different structures which were to be synthesized or obtained for the purpose of operating as ion conducting membranes.

This report summarizes work carried out between July 1971 and June 1972 under NASA contract NAS3-15692 to conceive, synthesize, and characterize new solid ionic conductors. During the one-year study crystal chemical principles have been used to predict structures and specific compounds which might have the desired properties. In excess of twenty compounds were synthesized or obtained and screened for evidence of ionic conductivity at low temperature. Encouraging results have been obtained for many of these materials but the work has not been carried so far as to prove whether compounds which pass screening tests are good conductors of ions at low temperature.

The report comprises three sections. The Introduction includes a Background which briefly reviews the structural and theoretical ideas which are the basis for the search for new conductors. Also in the Introduction is the Technical Approach outlining the structure selection, application of NMR, conductivity and transport measurement. The final part of the Introduction is a general discussion of the crystal structure of the compounds studied. The second section on Results, and Discussion of Results, describes the screening tests and evaluates the results. A final section on Conclusions summarizes the report and describes modifications in the approach for an extended study.

II. INTRODUCTION

A. Background

Many requirements must be satisfied when searching for a practical solid electrolyte for use in rechargeable batteries with high energy and power density at temperatures below 200°C. The primary requirements are that:

1. It must conduct ions of reactants with sufficiently high oxidizing and reducing power to results in high energy density.

2. The ionic conductivity at operating temperature must be sufficiently high to allow high power density.

3. It should have negligible electronic conductivity.

4. It must be chemically stable with respect to the cell reactants, reaction products, and sealing components.

5. It should be mechanically rigid and form sound seals.

6. It must have sufficiently low porosity to prevent mixing of the cell reactants.

Although all of these requirements are essential for a practical system, the most critical problem that must be solved is to discover solids which can conduct desirable ions at a suitable level. Until the last decade, solid electrolytes were universally considered to have ambient-temperature conductivities at least five orders of magnitude lower than aqueous electrolytes. Such solids have very low conductivities at room temperature (less than 10^{-6} $ohm^{-1}cm^{-1}$) which severely limit the power densities that can be attained.

The discovery of extraordinarily high ionic conductivities in double melts of AgI and Ag_2S by Reuter and Hardel[1] stimulated interest in solid electrolytes which led to the discovery of other compounds with similarly high ionic conductivities at ordinary temperatures. The high atomic weight of the reactants and the low free energy of compound formation severely limits the energy density of batteries based on silver salts although many low energy density applications of these electrolytes are being developed. The discovery of the high sodium ion conductivity of beta-alumina by Yao and Kummer[2] has led to a renewed interest in solid electrolytes with high specific energy and high power density.

A great deal of progress has been made in recent years in understanding the crystal structures and transport mechanisms of ionic conductors. The motion of ions through solids requires the creation of defects (vacancies or

interstitials) and their subsequent migration through the structure. In cases where the defect concentration is small and the defects are simple, they can be treated as individual entities and these normal or Type I solids have very low conductivities at temperatures far below their melting points.

All solids known to possess anomalously large ionic conductivities at relatively low temperature fall into one or the other of two classes. One type is the highly nonstoichiometric solids in which interaction between the multitude of defects has given rise to an extended defect structure. These are known as Type II conductors and it has been suggested that the large conductivities are due to cooperative motion between the migrating ions or anomalously long jump paths along the extended defect. An example of a Type II solid is the oxygen ion conductor $Ca_xZr_{1-x}O_{2-x}$ studied by Carter and Roth.[3] The third class of ion conductors is Type III. In these solids there is multiplicity of near-equivalent sites to which the mobile cations have access. There is a liquid like character to the cation distribution and examples include the silver chalcogenides and beta alumina. The relation between structure and transport properties has been discussed in detail by Rice and Roth[4] in their recently developed free-ion theoretical model for ionic transport through ionic conductors.

B. Technical Approach

The only solid electrolytes that have been identified with transport properties which appear to satisfy the requirements for a high energy density high-power density ambient battery are members of the beta-alumina family. The initial objective of the program was to survey and test as large a number as possible of structure types and compounds for evidence of ion conduction at low temperature. The search required the establishment of crystal chemical criteria to arrive at a list of candidates, obtaining or synthesizing candidate materials, and the development of methods for their characterization.

Structure Selection

The search for structure types was guided by the ideas exposed in the Free-Ion Model of ion conduction.[4] The conductivity is considered to be determined primarily by three parameters: N, the concentration of potentially mobile carriers; E, the gap or activation energy; and ℓ_0, the mean free path or inverse lifetime of the conducting state. Accordingly the search was directed towards 1) maximizing N by selecting structures which contain large concentrations of the mobile ion, 2) minimizing E by incorporating the mobile ions in open framework structures with interconnected interstices or structures with a multitude of crystallographically equivalent sites per cation, 3) increasing ℓ_0 by choosing nonstoichiometric compounds which exist over a broad composition range and contain extended defects. The crystallographic literature was surveyed to generate a list of structures and compounds which appeared to satisfy one or more of these characteristics. Specific attention

was directed to identifying structures in which the interatomic distances were large compared to the sum of ionic radii, and structures in which there was evidence of large thermal vibrations or low temperature phase transitions. The list was then adjusted to maximize the number of structure types that would be surveyed and to satisfy thermodynamic criteria for stability.

NMR Screening

Essentially all compounds that are of interest have complex structures and frequently neither the composition nor phase diagram is known. Accordingly, the magnitude of the problem of synthesizing and fabricating a large number of pure materials was reduced by using nuclear magnetic resonance to screen for ionic mobility. This method has several advantages: it can be used with powders; it responds to the specific ion which conducts the charge; it is tolerant of impurities. NMR screening also has several disadvantages: short and long range motion cannot be distinguished and the screening provides only a necessary, but not a sufficient, condition for ion transport; its use is restricted to nuclei with appropriate nuclear moments. Fortunately many ions with good nuclear properties, particularly ^{1}H, ^{7}Li, ^{23}Na, and ^{19}F, are of particular interest in this study.

The NMR linewidth or spectrum structure may include effects from several mechanisms. These are primarily: nuclear quadrupole interactions, chemical shift, knight shift, and dipole-dipole interactions with like and unlike nuclei. The detailed analysis that would be required to take into account all of these mechanisms was not practicable in the complex structures being investigated. For screening purposes spectra were measured at two or more temperatures and line narrowing at increasing temperature was taken as evidence for ion motion. The simple observation of motional narrowing does not distinguish between local and long range motion such as would be necessary for the solid to be an ionic conductor.

Some of the motional narrowing curves have been analyzed in the framework of an unpublished semi-phenomenological theory by Hendrickson and Bray which deduces an activation energy for motion and a range parameter suggesting whether the motion is short or long range. Although the model appears to be too simple, and does not include several important contributions to the line widths, a few tentative analyses were made in the spirit of learning to assess its value.

The NMR spectra were measured by I. Chung, D. Kline, and H. Story of the Physics Department, State University of New York at Albany. A Varian Associates wide-line NMR spectrometer with signal averaging was the principal instrumentation. Specimens in the form of powders were packed into 9mm OD quartz tubes and sealed to avoid atmospheric contamination.

Electrical Conductivity

The conductivity of ionic conductors can be determined exactly but the measurement is associated with certain problems which restrict the methods which may be used. The major problem is that electronic instruments must be used to determine ionic movement and special methods must be devised to insure that the blocking interface does not affect the measurement. The method judged best for this investigation was a four probe, low frequency, a. c. technique. The use of four probes, two outer probes supplying a fixed current and two inner probes determining a potential drop, eliminates contact resistance at the inner probes. The use of very low a. c. current reduces polarization or blocking at the ion-electron probes. Phase locking must be provided to assure that only the in-phase component of conductivity rather than the dielectric component is determined.

An instrument suited for these functions in conductive samples is the Keithley model 503 milliohmeter. The instrument can be modified to read resistances higher than the rated 1000 ohm upper limit by attenuating the gain of the detector circuit. With this modification, reliable conductivity measurements are possible on solid ionic conductors with metallic contacts, such as cathode sputtered platinum, in samples approaching a resistance of 100,000 ohms.

Rough indications of conductivity in ionic conductors can be obtained with two probe high impedance d. c. ohmmeters, but only when the resistivities are very high or electrodes are supplied which provide a source of the transporting ions in the solid. It was often necessary to resort to d. c. measurements in this investigation and those results are to be considered less reliable. Reasonable agreement was obtained in cases where the d. c. and four probe a. c. techniques overlapped in samples with resistivities in the 10^4-10^5 ohm range.

Transport Measurement

The conductivity consists of the sum of the ionic and electronic transport. In looking for new solid electrolytes it is necessary to determine the fraction of current carried by ions. The method chosen was to establish different ionic activities at opposite ends of test samples and compare the theoretical electrochemical potential with the observed potential.

The experimental determination of the species which transport electric current in solids is a relatively difficult procedure, always involving indirect experiments and assumptions which are often not as safe as we would like them to be. In the search for new solid electrolytes the first transport number to be determined is that fraction of the total current which is carried by any ionic species as differentiated from any electronic species.

$$t_i = \frac{\sigma_i}{\sigma_i + \sigma_e} \qquad (1)$$

where t is the transport number, σ is the conductivity, and the subscripts i and e refer to ionic and electronic carriers respectively.

It is common practice to determine the transport number described above for materials such as calcia stabilized zirconia by establishing a different oxygen partial pressure at electrodes on different sides of the test electrolyte. This gives rise to a potential, E_0, and the ratio of this and the observed potential is the transport number

$$t_i = E/E_0 \, . \qquad (2)$$

This is often represented by the equivalent circuit of Fig. 1a. This circuit can easily be shown to be compatible with both equations 1 and 2. There is no lateral connection along the length of the conductors because this would be assuming that oxidation and reduction of ions occurs along the length of the solid. It is convenient for the rest of the discussion to split the symbol for the electrochemical cell into two half cells as in Fig. 1b. f is an arbitrary number which will drop out of the final result, so we need not be concerned with its value or significance, other than it is a way to split the symbol for a cell into two half cells.

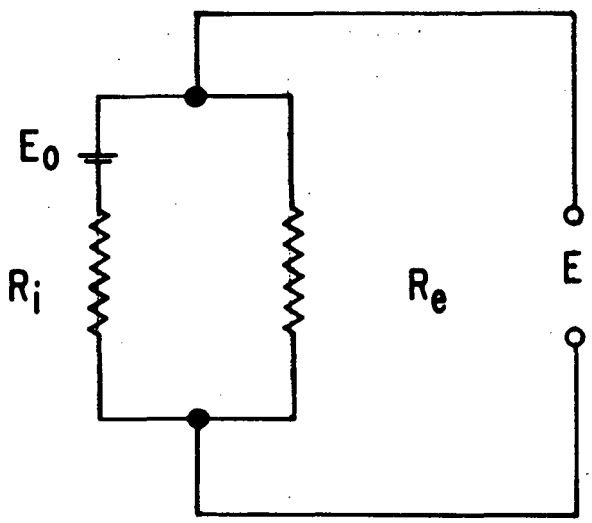

Figure 1a Equivalent circuit of a mixed ionic, electronic conduction where R_i and R_e are the ionic and electronic resistances.

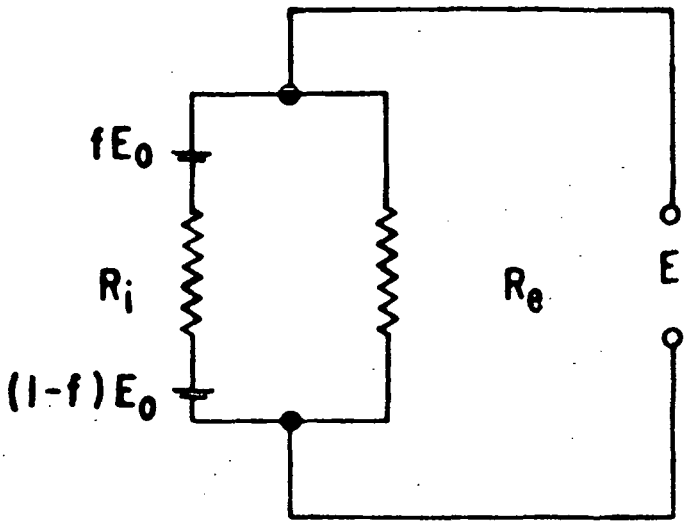

Figure 1b Circuit of Figure 1a where E_0 has been split into two half-cells by a fraction f.

It is important to note that the ionically conducting species in the solid need not be the same as that species which sets up the electrochemical potential. For instance MgO is predominantly a magnesium ion conductor at 1000°C and gives the theoretical potential as determined by an oxygen concentration difference. There need only be the possibility of equilibrium between magnesium and oxygen at the surfaces.

It is an obvious extension of this technique to study transport in solid electrolytes at room temperature, by employing typical battery electrodes to establish the potential E_0, for instance a nickel oxide battery plate, on one side with a cadmium plate at the other, both moistened with a hydroxide solution. If simultaneous electronic and ionic contact is made to the solid electrolyte, the circuits of Fig. 1 are applicable and the transport number is determined from E and E_0. However, there is a serious physical situation which may arise resulting in an erroneous result.

Consider how a purely electronically conducting solid connected as described could give an experimental E equal to E_0. For this situation to occur it will be assumed that poor, in fact no, electronic contact has been achieved between battery plates and the solid. Although ions will be blocked at the solid, "electrolyte" exchange reactions are possible at the liquid-solid interface and only partial blocking occurs. With high impedance voltage measuring instruments, the theoretical potential will be observed. If there is some corrosion or dissolution of the solid the exchange may be so rapid as to permit large currents to flow with no evidence of ion blocking. An equivalent circuit

of this electronic "electrolyte" between two battery plates with only liquid electrolyte contact is shown in Fig. 2a. In the figure the electron-ion exchange at the surfaces of the solid are represented by two equal and opposite half cells, ϵ_1 and ϵ_2. The consequences of this assumption will be discussed later. The liquid electrolyte resistance between fE_0 and ϵ_1, and between ϵ_2 and $(1-f)\ E_0$ has been neglected.

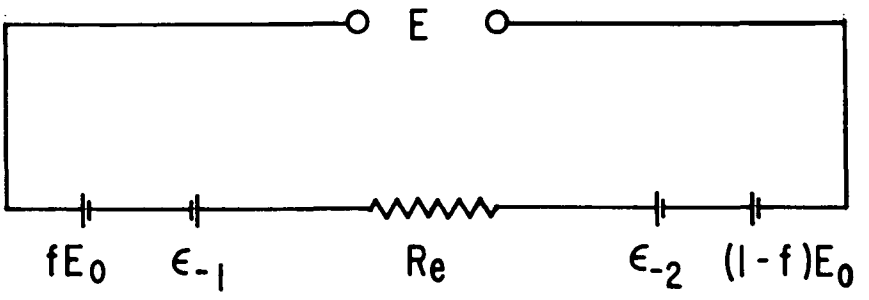

Figure 2a Electronic conductor, R_e between two battery plates. No electronic contact between plates and R_e.

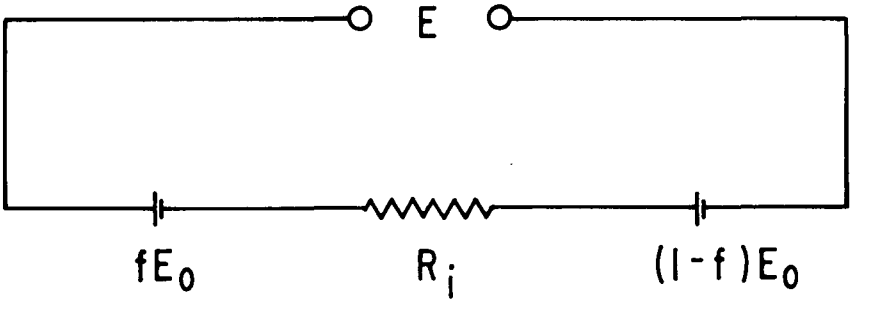

Figure 2b Ionic conductor, R_i, between two battery plates.

Figure 2b represents a solid ionic conductor in the same configuration again neglecting the liquid electrolyte resistance. Figure 2c is the parallel representation which is the equivalent of a mixed conductor. These were combined just as in Fig. 1 except for the condition of only ionic contact. When electronic contact is absent a mixed ionic-electronic conductor between two battery plates will give an open circuit potential representative of Fig. 2c rather than Fig. 1b. It is obvious that all the circuits of Fig. 2 yield $E = E_0$ under the assumption of $\epsilon_1 = -\epsilon_2$.

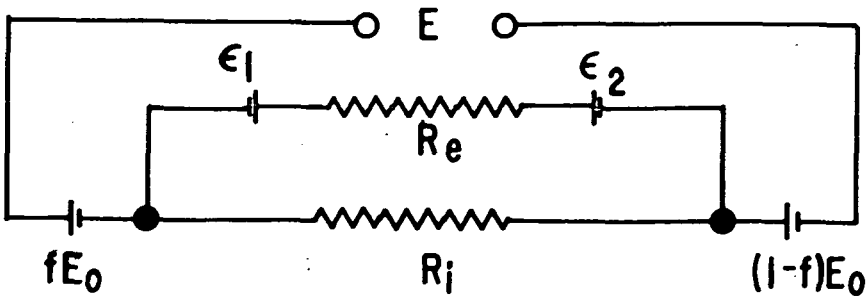

Figure 2c Mixed conductor between two battery plates. No electronic contact.

It is experimentally difficult to insure that good electronic and ionic contact are made at the same area of the samples. Adequate electronic contact is not possible in cases where the solid is being corroded or dissolved by the liquid. Good contacts of both types are made if the sample has the shape of a long bar or rod, making ionic contacts between the battery plates and the sample at the ends through a porous insulator moistened with liquid electrolyte. Electronic contacts can then be made away from the liquid toward the center of the sample. This is illustrated in Fig. 3a. The assumption is made that there will be no ion-electron exchange at the inner metallic electrodes, which is a good assumption in the absence of any liquid electrolyte at these points. Cadmium reference electrodes are included to test the assumption that $\epsilon_1 = -\epsilon_2$.

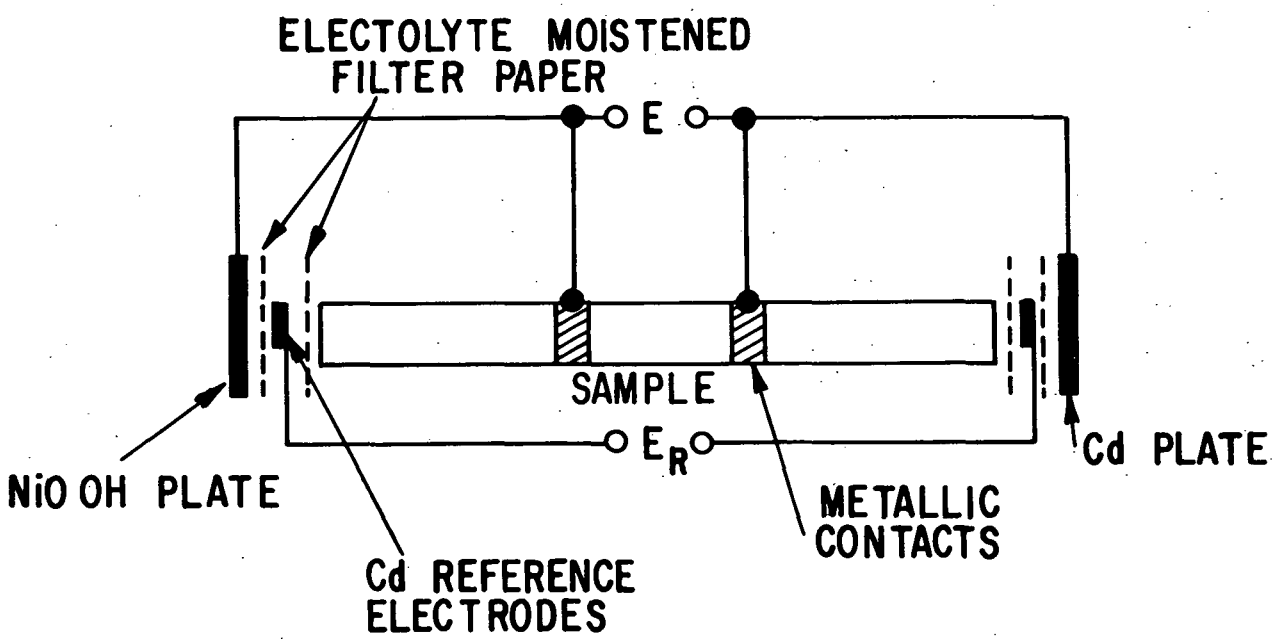

Figure 3a Schematic transport arrangement.

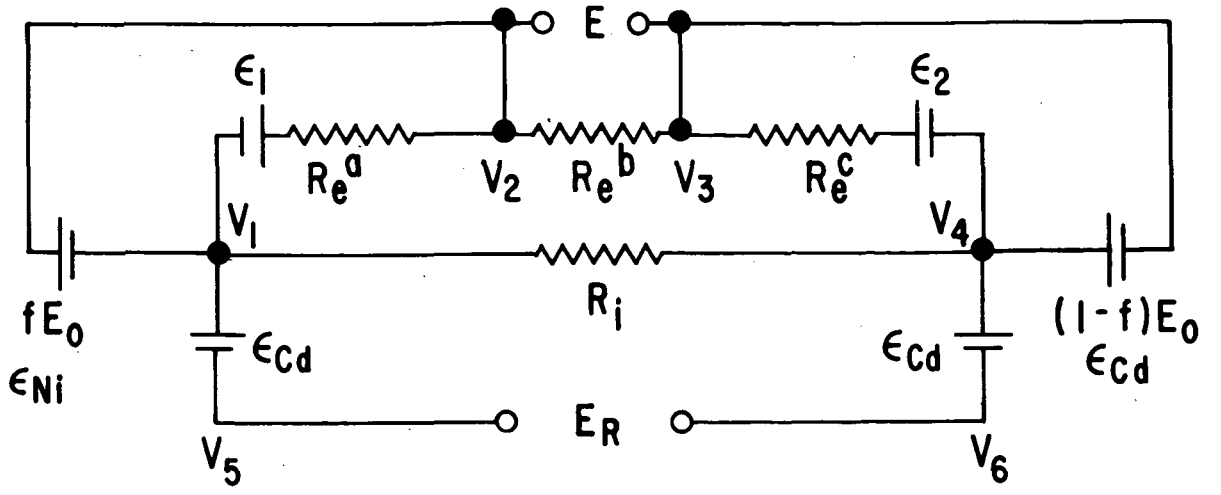

Figure 3b Equivalent circuit for Figure 3a.

The complex equivalent circuit of Fig. 3b need not be completely solved to extract relevant information. It is necessary from Kirchhoff laws that the current through R_i be equal to the current through R_e^b. From this fact it is possible to conclude that the transport number for ions may be determined by measurement of E, E_R, E_0, and the geometry of the sample. The current between points V_2 to V_3 and V_4 to V_1 dictates that:

$$\frac{R_i}{R_e^b} = \frac{V_4 - V_1}{V_3 - V_2} \tag{3}$$

V_4 and V_1 cannot be measured directly but the measurement at the reference electrodes V_5 and V_6 must be equal to their difference so that:

$$\frac{R_i}{R_e^b} = \frac{E_R}{E} \tag{4}$$

Assuming a homogeneous sample:

$$\frac{R_e^b}{R_e} = \frac{\ell}{L} \tag{5}$$

where $R_e = R_e^a + R_e^b + R_e^c$, L is the total length of the sample in Fig. 3a and ℓ is the distance between the center metallic electrodes,

$$\frac{R_i}{R_e} = \frac{E_R \ell}{E \cdot L} \tag{6}$$

$$t_i = \frac{1}{1 + (E_R \cdot \ell / E \cdot L)} . \tag{7}$$

From the above analysis it becomes apparent that the assumption of $E_1 = -E_2$ was not necessary. These voltages can only be generated in the electronic circular paths at each end of the equivalent circuit given so that E_1 and E_2 may have any value without affecting E and E_R. This being the case it is not necessary to incorporate reference electrodes because E_0 must equal the sum of E and E_R; and equations 6 and 7 become:

$$\frac{R_i}{R_e} = \frac{(E_0 - E)\ell}{(E)\, L} \tag{8}$$

$$t_i = \frac{1}{1 + \frac{E_0 - E}{E} \frac{\ell}{L}} . \tag{9}$$

If significant contact resistances are in the circuit at points V_1 and V_2 the above analysis is not applicable.

C. Crystal Structures

In excess of twenty crystalline solids were screened during this study for evidence of ionic mobility at low temperature. Many of the structures are not known or have been determined only approximately and in some cases the atomic arrangement can only be inferred from crystal chemical principles and analogy. This section gives a brief description of the atomic arrangement in the phases that were screened and comments on reasons for their selection. In subsequent sections these expectations are compared with the screening results and suggestions made to improve the reliability of predictions.

Li_3AlN_2

The structure of lithium aluminum nitride was determined by Juza and Hund[5] from x-ray intensity data obtained on powders. The compound crystallizes in a cubic cell with lattice parameter a = 9.46Å. The cell contains 16 Li_3AlN_2 molecules distributed in eight fluorite-like units. The 32 nitrogen atoms are in the face centered positions of the fluorite structure and 48 lithium and 16 aluminum atoms are arranged in an ordered fashion in the tetrahedral sites of the metalloid lattice. The bonding is strongly polar and the interatomic distances are compatible with the assumption of Li^{+1}, Al^{+3}, and N^{-3} ions. The structure is distorted and the atoms are displaced from the ideal fluorite positions such that the Li-N bond is 2.15Å, about 14% greater than the Al-N bond distance.

The crystal may be regarded as an antifluorite arrangement built of cubes of metal atoms which are joined by sharing edges. Adjacent cubes are either occupied by nitrogen atoms or are empty. The structure is similar to those of the stabilized zirconias which are excellent anion conductors.[2] Considering calcia stabilized zirconia $Ca_xZr_{1-x}O_{2-x}$ as an example, the nitrogens are distributed among the (Ca, Zr) sites and the (Li, Al) among the (O, vacancy) sites. Lithium migration in stoichiometric Li_2AlN_2 could occur by lithium hopping into vacant cubic sites not occupied by nitrogen. If lithium aluminum nitride can be made nonstoichiometric, both vacancy and interstitial transport mechanisms are possible and the phase could be a Type II conductor.

Li_3BN_2

The structure of lithium boron nitride has not been determined but the similarity of the chemical composition suggests it might be related to that of lithium aluminum nitride. This assumption is highly tenuous because the crystal chemistry of boron tends to be unique. The x-ray patterns of the aluminum and boron compounds are different and the infrared spectrum of the latter has been reported to show $(N = B = N)^{-3}$ ions in the crystal.[6]

Despite the above reservations, lithium boron nitride will be regarded as a distorted antifluorite similar to lithium aluminum nitride. The potential conduction mechanisms are the same as those discussed for that compound with the further possibility that the covalency of the B-N bond may promote the formation of extended defects with long mean free paths for lithium in the free-ion state.[4]

$LiAl_5O_8$

Several forms of lithium aluminate[7, 8, 9] have been reported but the structural relationship between them is not entirely clear. The equilibrium high temperature form is a cubic spinel with a = 7.921Å. The distribution of cations is not definitely established but x-ray intensities favor an inverse arrangement $Al_2[LiAl_3]O_8$ with lithium and aluminum distributed at random among the octahedral sites. The oxygen atoms in spinel are essentially close packed and migration of lithium at low temperature would not be expected.

Datta and Roy found that nitrate gels when dehydrated at temperatures below 1295°C form nonspinel metastable phases with different types of disorder. X-ray patterns of the metastable phases could be indexed on a cubic cell but reflections were observed that are not allowed by the spinel arrangement. These forbidden reflections could be explained if the cations were partially ordered. Disordered phases are difficult to characterize with powder diffraction patterns. It may be that metastable lithium aluminate is nonstoichiometric and contains cation vacancies, analogous to γ - Al_2O_3 which has the spinel arrangement with vacancies in aluminum sites: $Al_{21\ 1/3}\square_{2\ 2/3}O_{32}$. The $LiAl_5O_8$ composition is the same as rhombohedral beta alumina (β'' or 3-

block) in which spinel-like blocks are separated by planes with an open network of sodium and oxygen ions through which sodium migrates readily.[10] If metastable lithium aluminate were nonstoichiometric lithium ions and vacancies might develop short or long range order similar to that in β''-alumina through which easy migration of lithium could occur.

$LiNb_6O_{15}F$

The crystal structure of lithium niobium oxyfluoride is known from three dimensional single crystal data.[11] The structure is a polygonal network which contains building blocks each consisting of a pentagonal bi-pyramid NbO_5 sharing edges with five NbO_6 octahedra. There are tunnels between the $Nb_6O_{15}F$ building blocks which are large enough to contain the lithium ions. Within the tunnels are two sets of reasonable positions for lithium, either of which give rise to lithium-anion contacts ranging from 2.5Å to 3.0Å. These distances are quite large when compared to the sum of the ionic radii, $R(Li^{+1}) + R(O^{-2}) = 2.10$Å, and there may be easy mobility of lithium ions in the tunnels. An attractive feature of this material is electronic conductivity will probably be absent since there is complete charge compensation and the niobium is present in the +5 state.

$Li_xV_2O_5$

The Li_2O-VO_2-V_2O_5 system is complex and only the major features of the structures in different regions of the composition diagram have been established. An initial systematic study[12] showed three phases, α, β, and γ, each existing over a wide range of composition.

$0 < x \leq 0.13$	α
$0.13 < x < 0.22$	$\alpha + \beta$
$0.22 \leq x \leq 0.62$	β
$0.62 < x < 0.88$	$\beta + \gamma$
$0.88 \leq x \leq 1$	γ

A reinvestigation[13] has shown the β phase is stable only to $x = 0.37$ and that from $x = 0.44$ to 0.49 there is a closely related β' phase with diffraction pattern very similar to that of β. The β and β' phases appear to coexist over the range $0.37 < x < 0.44$.

The α phase is orthorhombic and for composition $x = 0.04$ the bimolecular cell parameters are $a = 11.460$Å, $b = 3.55$Å, and $c = 4.368$Å. The structure is nearly identical to that of V_2O_5 and the α phase is essentially a solid solution of Li_2O in V_2O_5. The most likely positions for lithium atoms indicate moderately large Li-O distances of order 2.10Å to 2.45Å.

The β phase is monoclinic with a 6 molecule cell of dimensions a = 10.03Å, b = 3.60Å, c = 15.38Å, β = 110.7°. The VO_6 octahedra are linked to form a network containing tunnels in which lithium ions are distributed. In the β structure the lithium ions appear to be randomly distributed among two sets of sites. There are eight coordinated sites, tetrahedrally coordinated sites and octahedrally coordinated sites within the tunnel. Single crystal analysis[13] indicates that the various phases may differ primarily by the distribution of lithium ions in the tunnels.

The availability of a large number of sites with nearly equal energy suggests $Li_xV_2O_5$ compounds are potential Type III conductors with lithium ions migrating easily along the tunnels.

$Li_xTa_2O_5$ and $NaTa_5TiO_5$

The existence of a number of compounds in the Li_2O - Ta_2O_5 has been established by powder diffraction patterns but their structures have not been solved. Reisman and Haltzberg[14] found three phases Li_3TaO_4, $LiTaO_3$, and $LiTa_3O_8$ in materials prepared at $Li_2Ta_4O_{11}$ by reaction at 900°C and found it decomposed into $Li_2Ta_8O_{21}$ + Li_2O at 1400°C. The compositions $LiTa_3O_8$ and $Li_2Ta_8O_{21}$ probably refer to the same phase. At small concentrations of lithia an orthorhombic phase is formed which probably is a solid solution of Li_2O in Ta_2O_5.

The atomic arrangements of the tantala-rich compounds are expected to be related to the tunnel structures which are formed in the niobates (see discussion above $LiNb_6O_{15}F$). This view is supported by x-ray analyses which show $Na_2Nb_4O_{11}$ and $CaTa_4O_{11}$ contain analogous layers of pentagonal niobium (tantalum) oxygen bipyramids arranged in essentially the same way.[16] Jahnberg also found that attempts to prepare $Na_2Ta_4O_{11}$ reported by Whiston and Smith and Reisman gave a material with a powder pattern that closely resembled that of $Na_2Nb_4O_{11}$ and $CaTa_4O_{11}$.

Compounds in the Li_2O-Ta_2O_5 and Na_2O-Ta_2O_5 system are expected to crystallize in tunnel structures along which there could be easy migration of M^+ ions. Nonstoichiometric compounds in these phases may be electronic conductors but if the postulated compound "$NaTa_5TiO_{15}$" is stable the structure would be charge compensated and a purely ionic conductor.

$NaCaPO_4$

Sodium calcium phosphate crystallizes in a low temperature form with the orthorhombic K_2SO_4 arrangement.[17] The pseudo hexagonal cell with a = 6.830Å, b = 5.215Å, c = 9.320Å contains 4 molecules in an open packing of Na^+ and Ca^{++} cations with tetrahedrally coordinated $PO_4^{=}$ anions. The phase transforms at 680°C into a high temperature modification containing 2 molecules in a hexagonal cell with parameters a = 5.36Å, c = 7.33Å.

The low to high transition is accompanied by an increase in symmetry and disorder due to rotations or displacements of the phosphate groups. The transition is associated with a 5% decrease in density. Since Ca^{+2} ions are probably immobilized by their larger charge and size, the Ca^{+2} and PO_4^{-2} groups may form an open framework with sufficiently large interstices for sodium migration.

Na_2BeF_4

Sodium beryllium fluoride crystallizes in the same orthorhombic K_2SO_4 structure described for sodium calcium phosphate. The low temperature lattice parameters are a = 6.560Å, b = 4.892Å, c = 10.900Å and the hexagonal parameters of the high temperature modification are a = 5.31Å, c = 7.08Å. Structural transformations in Na_2BeF_4 occur at 115°, 225°, and 320°C and sodium ion migration might be possible at these temperatures if there are large enough interstices between the tetrahedral BF_4^{-2} ions.

K_2TiF_6

K_2TiF_6 is a member of a group of complex fluorides of formula A_2BF_6 which occurs in three structure types typified by K_2SiF_6 (cubic), K_2GeF_6 (trigonal) and K_2MnF_6 (hexagonal).[18] The structures are built up of close packed layers of K and F with the small cations in certain octahedral holes. α-K_2TiF_6 is cubic close packed with a = 8.32Å, β-K_2TiF_6 is double hexagonal close packed with a = 5.75Å, c = 9.46Å, and γ-K_2TiF_6 is hexagonal close packed with a = 5.715Å, c = 4.656Å.

Since each Ti atom is linked to six F atoms at the corners of a distorted octahedron, the structures alternatively may be regarded as different packings of K^{+1} and TiF_6^{-2} ions. From this point of view, the α form has the anti-fluorite structure in which the TiF_6 octahedra and K atoms are distributed in the same manner as calcium and fluorine in CaF_2. The γ form has a structure which resembles CdI_2 and is layerlike. If the interstices in the layer are sufficiently open, two dimensional migration of alkali ions between the layers of titanium hexafluoride octahedra may be possible.

$NaBO_2$

Sodium metaborate crystallizes in a rhombohedral cell with lattice parameters z = 7.22Å and α = 110°29' which contains 6 $NaBO_2$ molecules. The structure is composed of Na^{+1} and planar $(B_3O_6)^{-3}$ ions which are formed by linking boron and oxygen atoms in a ring.[19] The sodium ions occupy the interstices between large $(B_3O_6)^{-3}$ groups and have an unusual coordination number equal to seven. The average Na-O distance is 2.53Å which might be sufficient to permit diffusion of sodium ions.

$NaLaF_4$

Sodium lanthanum fluoride crystallizes in a hexagonal cell with a = 6.155Å, c = 3.811Å and is reported to have the β-$NaThF_6$ structure with 3/2 molecules in the unit cell. A single crystal x-ray analysis has established the structure of the isomorphous compound $NaNdF_4$.[20] Fluoride ions lie in triangular arrays in layers perpendicular to the hexagonal axis and there are three types of cation sites: a one-fold site occupied by $Nd^{+3}(La^{+3})$, a one-fold site occupied randomly by $1/2Na^{+1}$, $1/2Nd^{+3}(La^{+3})$, and a two-fold site occupied randomly by Na^{+} and vacancies. The thermal vibration ellipsoids of the fluorine atoms and the sodium ions which occupy the two-fold sites are anomalously large and anisotropic. The Na-F distances are not particularly large, ranging from 2.298Å to 2.459Å, but in view of the excessive disorder this structure may be considered a reasonable candidate for ion conduction.

$NaF-LnF_3$

Phase diagrams for the sodium-lanthanide rare earth fluoride binary systems typically show hexagonal phases similar to $NaLaF_4$ discussed previously and cubic phase regions which extend over a range of composition.[21] The cubic phases are fluorite-like and substitution of Ln^{+3} into the fluorite unit cell gives rise to cation vacancies which can be partially compensated by fluoride ions in interstitial positions.[22] As the temperature is lowered the cubic phase undergoes solid state transitions to an orthorhombic phase which appears to be a superstructure based on the fluorite lattice. The structure situation is extremely similar to that in the stabilized zirconia and these materials appear to be excellent candidates for Type II ion conduction.

Zeolite Frameworks

Zeolites can be defined as crystalline aluminosilicates with framework structures which enclose cavities occupied by large ions and water molecules. The zeolite structures are complex and represent a broad spectrum of compounds which include the sodalite family as one of the major groups. Typical unit cell compositions of hydrated X and Y zeolites and a faujasite crystal are as follows:

$$X\ Na_{86}\ [(AlO_2)_{86}\ (SiO_2)_{106}],\ 264\ H_2O$$

$$Y\ Na_{56}\ [(AlO_2)_{56}\ (SiO_2)_{136}],\ 250\ H_2O$$

$$Faujasite\ Na_{12}Ca_{12}Mg_{11}\ [(AlO_2)_{59}\ (SiO_2)_{133}],\ 235\ H_2O$$

The structures of many zeolites consist of simple arrangements of polyhedra; each polyhedra itself is a three-dimensional array of (Si, AlO_4) tetrahedra in a definite geometric form. In a typical A-type zeolite, there are internal cavities 11Å in diameter which are interconnected by circular apertures with free diameters of 4.2Å. When hydrated the cavities are filled

with water molecules and hydrated salts. When the water is removed the ions are found bound on the walls of the cavities.

III. RESULTS AND DISCUSSION OF RESULTS

This section is arranged so that all results and discussion are given as separate groups for each compound. Primary emphasis of the work was screening of a large number of compounds, therefore, some materials have not been carried through the experimental procedures of fabrication, conductivity, and transport measurement.

Li_3AlN_2

Sample Preparation

98% pure Li_3N and 99% pure AlN were mixed in a closed jar to reduce reaction with water vapor, then fired in a molybdenum crucible in a N_2 atmosphere. The temperature was slowly increased to 780°C in five hours and held constant for 16 hours. The reaction product was ground under nitrogen and stored in a vacuum equipped with a nitrogen cold trap. X-ray examination showed the product was principally Li_3AlN_2 plus a less amount of AlN.

The powder was pressed at 5000 pounds pressure in a 3/16" x 2" die, transferred to a furnace with a nitrogen atmosphere within a few minutes and then fired at 900°C. The pressed and fired bars were very poorly sintered and too fragile to measure their density. NMR samples for this composition and all other compounds were prepared by sealing the powders in 10 mm diam. evacuated quartz tubes.

NMR Screening

The NMR absorption mode spectrum of ^7Li consisted of a single line at the unperturbed resonant frequency plus two pairs of first-order satellites. The central line undergoes motional narrowing in the temperature range from -160°C at +265°C as shown in Table I. The rigid lattice line width is achieved only at temperature below -100°C and there is strong motional narrowing at room temperature.

These data show there is at least strong local motion of lithium nuclei in lithium aluminum nitride at room temperature and below. A Hendrickson-Bray curve obtained on the basis of a computer best fit of the line width as a function of temperature is shown in Fig. 4. The analysis gives an activation energy of 2300 cal/mole and a range parameter of 0.1 gauss which suggests the motion is primarily local. Since the stoichiometry was not adjusted and dopants were not introduced, there is presently no reason for the phase to have a large concentration of defect sites which is essential for high conductivity. The small value of the apparent activation energy indicates that lithium aluminum nitride might be an excellent conductor of lithium ions at low temperature if prepared as a nonstoichiometric compound.

TABLE I

Temperature Dependence of NMR Spectrum of ^7Li in Li_3AlN_2
ν_0 = 28.0 MHz

Temperature (± 2°C)	Peak-to-Peak Width (gauss)
-160	10.5 ± 0.3
-107	9.7 ± 0.3
- 80	8.5 ± 0.3
- 30	8.5 ± 0.3
RT	6.5 ± 0.2
80	3.3 ± 0.2
202	2.0 ± 0.2
265	1.5 ± 0.2

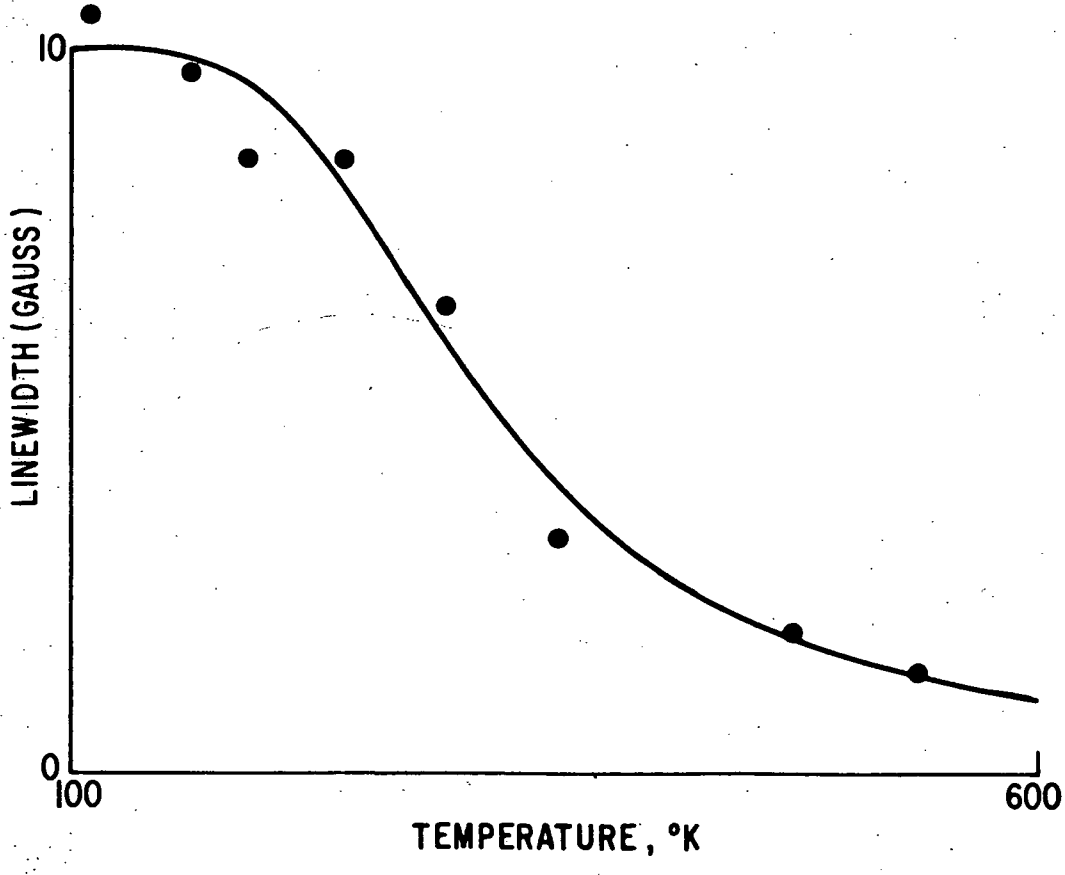

Figure 4 Temperature dependence of ^7Li NMR spectrum in Li_3AlN_2.

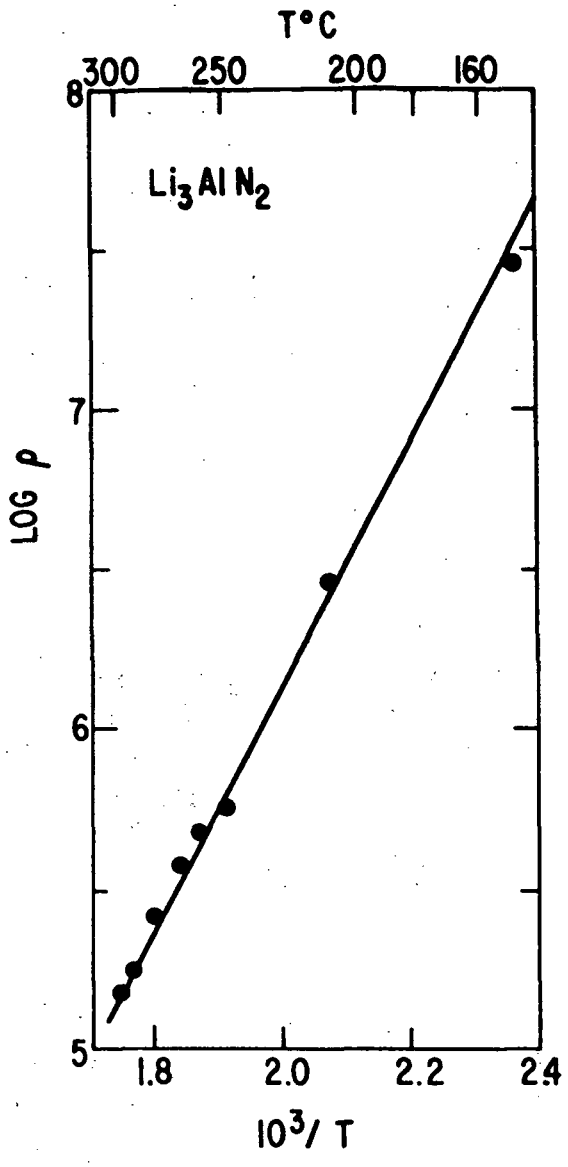

Figure 5 Log resistivity vs reciprocal temperature for Li_3AlN_2.

Conductivity

Figure 5 shows the temperature dependence of the resistivity of the lithium aluminum nitride specimen. The activation energy is 17,000 cal/mole. Since the test bar was multiphase and of low density, the conductivity result is not considered representative of pure Li_3AlN_2 and the large activation energy is probably due to grain boundary resistance.

Li_3BN_2

Sample Preparation

Lithium boron nitride was synthesized by R. C. DeVries and J. F. Fleischer of this Laboratory.[23] Lithium nitride from Lithium Corporation of America and boron nitride from Gallard Schlesinger Chem. Mfg. Corp. in a weight ratio of 1.403:1 were milled under a cover of dry nitrogen gas. The mixture was heated in a molybdenum crucible under a nitrogen atmosphere from R. T. to 600°C at 200°C/hour, from 600° to 750°C at 50°C/hour, then held at 750°C for one hour. A readily crushed powder was obtained which was protected from the atmosphere by storing under nitrogen.

Bars, 3/16"-square by 2" long, were fabricated for conductivity tests. Two methods were used: die pressing at 8000 pounds and firing at 825°C in N_2 for 16 hours; and die pressing at 8000 pounds, followed by hydrostatic pressing at 200,000 psi and the same firing conditions. In spite of the extremely high compaction pressure in the second method, neither procedure resulted in a well sintered body.

NMR Screening

The structure of lithium boron nitride is related to that of lithium aluminum nitride and hence is expected to conduct lithium for similar reasons. As expected, motional narrowing of the ^7Li NMR spectrum was observed in the temperature range from -140°C to room temperature. However, the spectrum is more complex and there are two Li resonance peaks, one showing a substantial decrease in line width from its rigid lattice value at approximately -100°C while the other does not substantially decrease until -20°C (Fig. 6). The temperature dependence of the latter spectrum is similar to that reported for one of the ^7Li sites in Li_3N by Bishop et al.[24] There was no evidence for lithium ions diffusing in Li_3N at temperatures as low as -100°C.

The Li_3BN_2 sample also gave a weak proton spectrum at room temperature, probably due to contamination with bound H_2O. This is consistant with the extremely hygroscopic nature of lithium boron nitride. It is not presently known whether the two lithium peaks are to be attributed to different sites in Li_3BN_2 or whether one should be associated with a hydration product.

Conductivity

Conductivity measurements were made in a vacuum and the results are summarized in Fig. 7. Four probe measurements were made at temperatures above about 200°C. At lower temperatures it was necessary to make two probe measurements for which there was evidence of appreciable contact resistance. The more reliable high temperature four probe results show an activation

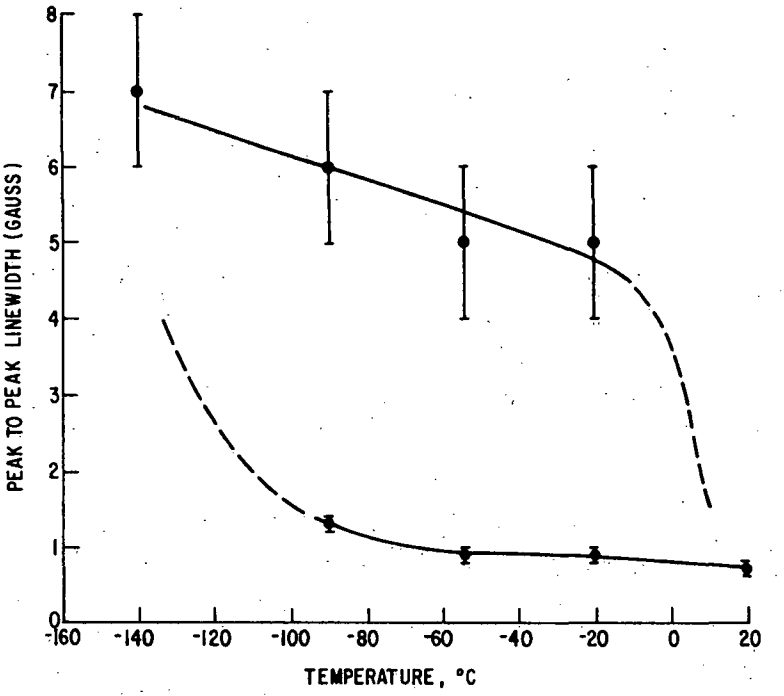

Figure 6 Temperature dependence of ^7Li NMR spectrum in Li_3BN_2. The spectrum has two peaks, one of which shows a substantial decrease in line width from its rigid lattice value at approximately -100°C, the other at approximately -20°C.

energy of 10,000 cal/mole to be compared to 15,000 cal/mole obtained from the two probe measurements. Because of the low density and doubtful purity of the samples, the values of conductivity are very uncertain.

$LiAl_5O_8$

Sample Preparation

Lithium meta aluminate was prepared by decomposition of a mixture of $LiNO_3 \cdot 3H_2O$ and $Al(NO_3)_3 \cdot 9H_2O$ in a platinum crucible. The molten salts were stirred to insure intimate mixing and heating was continued to 1280°C for 16 hours in air. The resulting partially sintered cake was ground and stored in a vacuum. X-ray diffraction showed the product was an approximate 50% mixture of the nonspinel form of cubic $LiAl_5O_8$ reported by Datta and Roy[8] and γ-$LiAlO_2$.

NMR Screening

The NMR absorption spectrum showed a single ^7Li line at the unperturbed resonance frequency. The line width was measured from -160°C to +262°C with the results given in Table II.

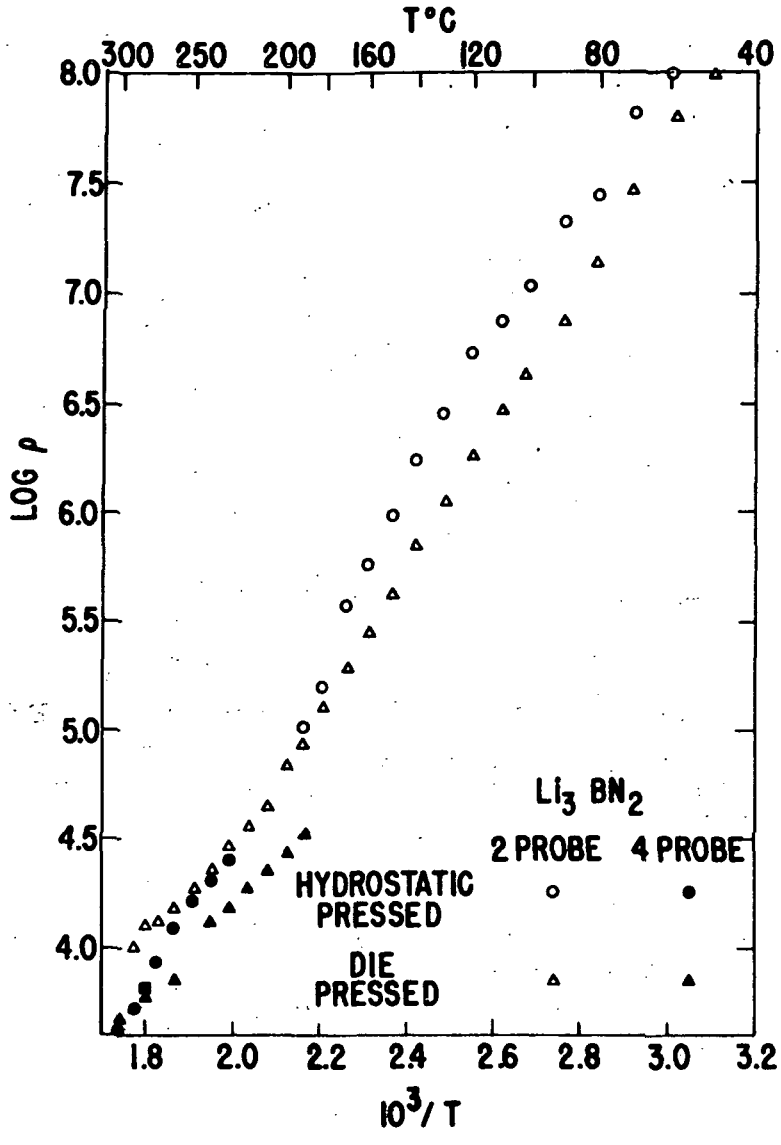

Figure 7 Log resistivity vs reciprocal temperature for Li_3BN_2.

TABLE II

Temperature Dependence of NMR Spectrum of ^7Li in $LiAl_5O_8$
ν_0 = 20.0 MHz

Temperature (±2°C)	Peak-to-Peak Width (±0.3 gauss)
-160	4.7
RT	4.1
+205	4.2
+262	3.9

There is only a small effect of temperature on the ^7Li line width and it is tentatively concluded $LiAl_5O_8$ shows little promise of being a good ion conductor at low temperature. This conclusion is limited by the following proviso. The specimen contained a mixture of $LiAl_5O_8$ and $LiAlO_2$ and thus observed absorption consists of at least two peaks which originate from lithium ions in different phases. Strong motional narrowing of lithium in $LiAl_5O_8$ could have been masked by the wide rigid lattice line widths of lithium in $LiAlO_2$.

Conductivity

The resistivity of a sintered bar of the $LiAl_5O_8$ - $LiAlO_2$ mixture was 10^8 ohms at 300°C and a ρ-T plot was not obtained. The bar was less than 60% dense but the resistivity is so high that completely dense material of this composition would also show very low ionic conductivity.

$LiNb_6O_{15}F$

Sample Preparation

Lithium niobium oxyfluoride was synthesized following the procedure described by Lundberg.[11] LiF and Nb_2O_5 were milled for 16 hours and fired in a platinum crucible at 1200°C for 20 hours in argon. X-ray diffraction showed the phase predominantly $LiNb_6O_{15}F$ although a few extraneous lines were present that could not be identified.

NMR Screening

A single, symmetric line was observed for ^7Li in the NMR spectrum of lithium niobium oxyfluoride. Table III gives the line widths measured from -170° to +183°C. Motional narrowing is observed which signifies at least short range motion of lithium at moderate temperature. The spectra obtained at room temperature at two different radiofrequencies, 28.0 MHz and 16.0 MHz, have the same line width within the error limit. The symmetrical line and the absence of a frequency dependence are characteristic of dipolar broadening only. The absence of a Knight shift suggests that if the material is a good ionic conductor the electronic component is small.

Figure 8 shows the line width as a function of temperature. The curve is drawn for parameters computed to give the best fit to the Hendrickson-Bray theory. These data yield a value for the activation energy of E = 3700 cal/mole and a range parameter B = 0.014 gauss. On the basis of their model, the low value of E and this range of value of B suggests the motion is primarily local. This result is not unexpected because x-ray measurements indicated the material was well crystallized and single phase and probably had only a small defect concentration.

TABLE III

Temperature Dependence of NMR Spectrum of ^{8}Li in $LiNb_6O_{15}F$
ν_0 = 28.0 MHz

Temperature (°C)	Line Width (gauss)
-170	4.25 (±0.25)
-149	4.25 (±0.25)
-114	4.1 (±0.3)
- 85	4.5 (±0.5)
- 68	4.2 (±0.3)
- 26	3.6 (±0.3)
RT	3.0 (±0.2)
RT	*3.0 (±0.4)
108	1.7 (±0.1)
126	1.3 (±0.1)
183	0.6 (±0.1)

*Measured at 16.0 MHz.

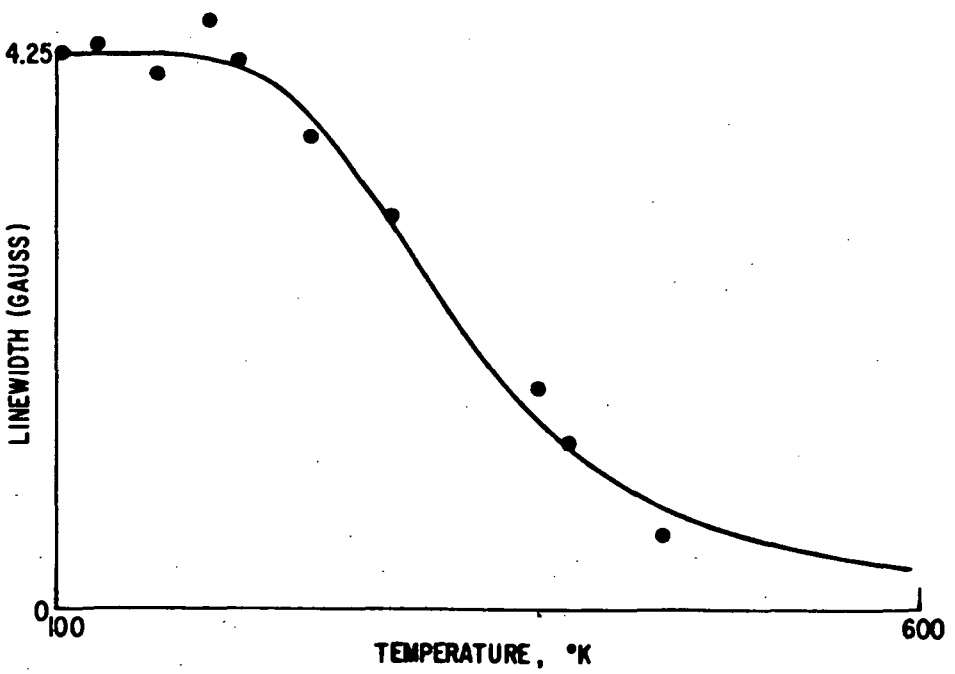

Figure 8 Temperature dependence of ^{7}Li NMR spectrum in $LiNb_6O_{15}F$.

$Li_xV_2O_5$

Sample Preparation

Three compositions with x equal to 0.1, 0.33, and 0.6 were synthesized using procedures similar to those of Kessler and Sienko[25] and Hagenmuller et al.[26] Starting materials were reagent grade Li_2CO_3 (Baker and Adamson), purified V_2O_5 Fischer Scientific) and 99% pure V_2O_3 (A. D. Mackay). Lithium metavanadate was first prepared in a platinum crucible at 1100°C by the reaction, $Li_2CO_3 + V_2O_5 = {}_2\ LiVO_3 + CO_2$. The reaction product was identified by x-rays to consist almost entirely of $LiVO_3$. $LiVO_3$ plus V_2O_3 and V_2O_5 were ground and mixed in the proper proportions to give the proper value of x, then heated under argon in platinum crucibles at 550°C for 18 hours. The products were ground a second time and again reacted at 550°C for 18 hours.

Five different techniques were used in attempting to obtain dense lithium vanadates. The most successful was hot pressing which produced a sample with open pore volume of 0.06%. No helium leak tight samples were fabricated.

(a) Sintering. Bar shaped samples were formed by pressing the powders and sintering. Parameters which were varied were: powder forming pressure, powder grinding times and methods, oxygen stoichiometry, and firing temperature. Densities were typically 50% to 80% of theoretical. The final densities were almost independent of the initial compaction, powder composition and particle size. The highest densities were obtained only by firing at temperatures high enough to form some liquid phase.

(b) Melting. By melting and cooling $Li_{0.33}V_2O_5$ in platinum containers small regions of theoretical density (a few square millimeters) were obtained at the surface in contact with the platinum. This method could be used to obtain pore free material by designing crucibles to accommodate the volume change on melting. X-ray diffraction showed the melted and sintered products were identical.

(c) Single Crystals. Slow cooling from the melt results in long needles (up to a centimeter) which are single crystals when a tenth of a millimeter or less in thickness.

(d) Composites. Molten $Li_{0.33}V_2O_5$ is quite fluid and wets alpha alumina. Several samples have been prepared by melting the vanadate with disks of porous alumina submerged in the melt. The composite suffers from the same volume change problem as in melting without the alumina and no helium leak tight material was produced. This problem could probably be solved and the method may find use as a practical solid electrolyte composite for solid electrolytes which have poor physical strength.

(e) Hot Pressing. Hot pressing of all three compositions has resulted in densities with less than 1.5% open pores. Samples were pressed, pressing at 7000 psi at 575°C using graphite dies.

NMR Screening

Three compositions of $Li_xV_2O_5$ with x = 0.1, 0.33, and 0.6 were screened for lithium mobility. The x = 0.1 composition lies near the lithium-rich end of the α phase region which extends from x = 0 to x = 0.13. The x = 0.33 and x = 0.6 compositions were selected to lie near the lithium-poor and lithium-rich extremes of the β phase to ascertain the effect of varying the concentration of lithium ions in the tunnels. X-ray diffraction showed the specimens were multiphase. The x = 0.1 composition was predominantly orthorhombic α but also contained a significant quantity of the monoclinic β phase. The x = 0.33 composition contained a smaller amount of α and was predominantly β. The x = 0.6 composition consisted of beta plus a lesser amount of γ and $LiVO_3$.

The ^7Li spectra of all three samples at room temperature are similar except the signal strength increased with lithium content. The ^7Li spectrum had an asymmetric line shape as shown in Fig. 9. The x = 0.33 composition was nearly single phase and the temperature and frequency dependence were studied in greater detail. Table IV gives the temperature dependence of the line width and the asymmetry ratio A/B of the ^7Li resonance. Table V gives the frequency dependence of the line width.

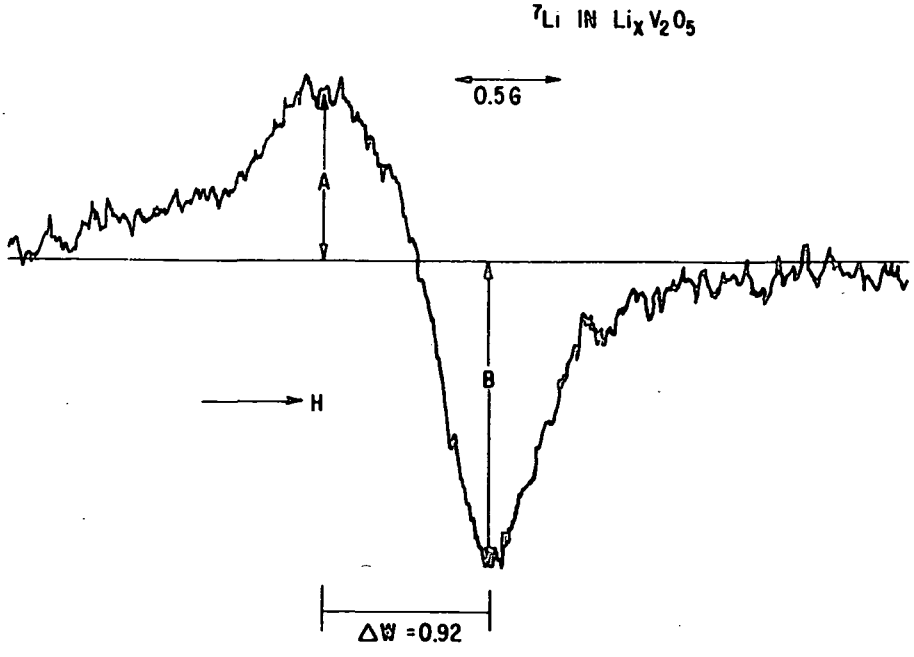

Fig. 9 ^7Li NMR spectrum in $Li_{0.33}V_2O_5$ the peak-to-peak line width ΔW = 0.92 gauss and the asymmetric line shape determined by the intensity ratio A/B are frequency dependent.

TABLE IV

Temperature Dependence of NMR Spectrum of ^7Li in $Li_{0.33}V_2O_5$
ν_0 = 28.0 MHz

Temperature (°C)	Peak-to-Peak Width (gauss)	Intensity Ratio A/B
-136	2.8 ± 0.2	1.0
-114	2.5 ± 0.2	0.84
- 89	2.0 ± 0.3	0.74
- 60	1.5 ± 0.2	0.59
22	0.92 ± 0.1	0.51
30	0.94 ± 0.04	0.58
62	0.78 ± 0.05	--
100	0.78 ± 0.05	0.59
140	0.60 ± 0.10	0.75
140	0.70 ± 0.20	0.70

TABLE V

Frequency Dependence of NMR Spectrum of ^7Li in $Li_{0.33}V_2O_5$
Room Temperature

Frequency (MHz)	Peak-to-Peak Width (gauss)
7.0	0.35 ± 0.04
10.0	0.40 ± 0.05
13.0	0.45 ± 0.05
16.0	0.50 ± 0.10
19.0	0.65 ± 0.05
29.0	0.90 ± 0.05

The asymmetry and frequency dependence are believed to be due to a Knight shift arising from interaction of conduction (s) electrons with the lithium nuclei. The shift is highly anisotropic which suggests both conduction electrons and lithium nuclei are moving in the tunnels of the β structure. Gendell et al.[27] looked for, but did not find, this effect in similar material.

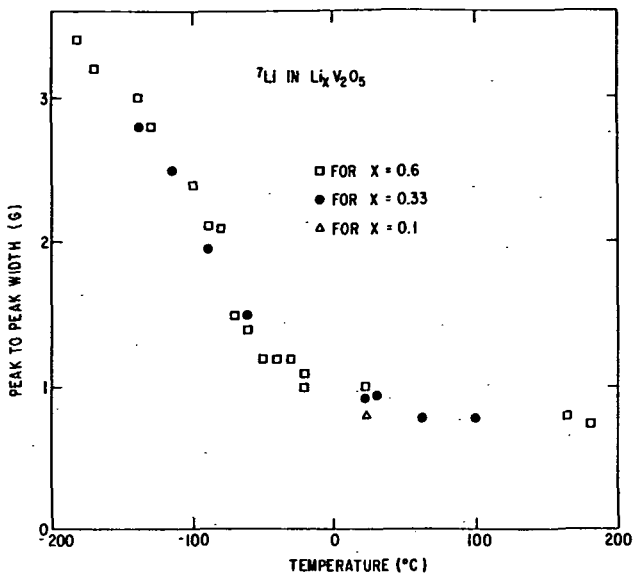

Figure 10 Temperature dependence of width of ^{7}Li NMR spectrum in $Li_xV_2O_5$.

In view of the multiphase nature of the specimens, these conclusions should be considered preliminary but they are supported by conductivity measurements which indicate appreciable electronic conductivity in the same materials.

The temperature dependence of the line widths of the three compositions are shown in Fig. 10. They are all similar and it is tentatively concluded each shows strong motional narrowing. The results may be dominated by the β phase component and further work would be required to determine whether lithium in the α phase also undergoes motional narrowing.

Electrical Conductivity

All samples of $Li_xV_2O_5$ exhibited high conductivity. As discussed later, a large fraction of this conduction may be by lithium ion transport although reports in the literature interpret the conductivity as completely electronic. Conductivity measurements were obtained on sintered bars, hot pressed disks, and composite Al_2O_3-$Li_{0.33}V_2O_5$ samples. None of the compositions were single phase. All measurements were made using the four probe technique.

Given on Table VI are conductivities and densities as the process variables of powder size (ball milling), V:O ratio, and firing temperature were altered. There are apparently no correlations between any of these factors.

TABLE VI

Density and Resistivity of $Li_{0.33}V_2O_5$ as a Function of Process Variables

Powder Preparation	Sintering Temperature °C	550	650	700
$Li_xV_2O_5$ (V:O > 1:2.5)	density % theor.	62.3	81.7	78.3
	R.T. resistivity ohm · cm	11.0	2.9	2.1
V:O > 1:2.5 (ball-milled)	density % theor.	51.4	51.0	76.0
	R.T. resistivity ohm · cm	3.6	1.9	2.0
V:O < 1:2.5 (V_2O_3 added)	density % theor.	62.2	63.0	70.4
	R.T. resistivity ohm · cm	5.8	3.3	11.3

Resistivity - reciprocal temperature plots are given in Figs. 11 and 12 for the three compositions studied. There is the expected remarkable increase in conductivity in hot pressed (~95% dense) over sintered (~80% dense) samples. Activation energies are in the 2000 to 6000 cal/mole range. The dependence of the conductivity on the composition was complex. Over the temperature range from 25° to 200°C there was a maximum in the conductivity and a minimum in the activation energy for the x = 0.33 composition. The curves for sintered samples (Fig. 11) are more accurate than those for the hot pressed samples (Fig. 12) because of instrumentation difficulties. Contact impedances interfered with the lower temperature values and not too much significance should be given to the change in slopes on the Arrhenius plots for compositions x = 0.33 or 0.6. Furthermore, it is difficult to rationalize a decreasing activation energy with increasing temperature as this is contrary to that expected with competing ionic and electronic conduction mechanisms. The most significant conclusion to be drawn from a comparison of Figs. 11 and 12 is that relatively minor changes in density can make order of magnitude changes in electrical properties. Theoretically, there should be only a 20% increase of resistivity in a 70% dense sample compared to a 100% dense sample of the same composition, assuming no grain boundary resistance.

Given on Fig. 13 is the electrical resistivity of a composite sample as a function of temperature. The resistivity is an order of magnitude higher than sintered sample of the same composition, a larger increase than we expected.

Transport

Samples of the composition $Li_{0.33}V_2O_5$ were tested for transport number at room temperature, both in the form of 70% dense sintered bars 2 inches long by 3/16" square and 96% dense hot pressed disks 3/16" thick and one

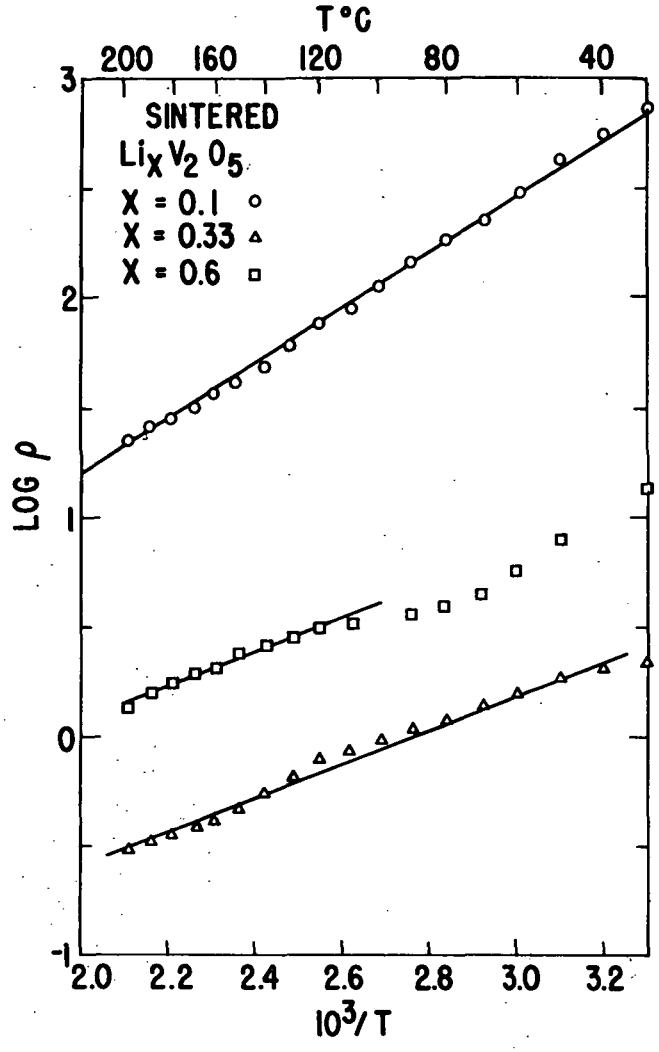

Figure 11 Log resistivity vs reciprocal temperature for sintered $Li_xV_2O_3$ with three different lithium contents.

inch in diameter. The method at first used was to apply sputtered platinum electrodes to both sides of the disk and both ends of the bars. Charged nickel and cadmium battery plates were then pressed to the platinized surfaces after being moistened with 10% NaOH or LiOH solutions. In all cases the open circuit potential corresponded to that for the Ni-Cd cell. On drawing current from the bar samples current vs voltage plots typically placed the overall resistance at 10^3 ohms, which was comparable to the a. c. resistance measurements of a few hundred ohms. On the other hand poor comparison was obtained between a. c. resistance and current vs voltage plots when using the hot pressed disk samples. Four probe a. c. resistance measurements

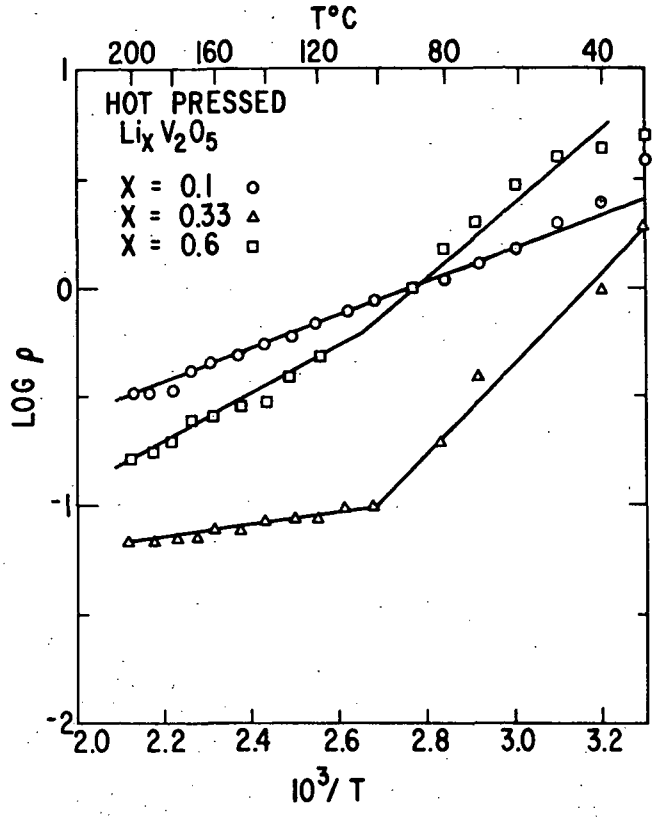

Figure 12 Log resistivity vs reciprocal temperature for hot pressed $Li_X V_2O_5$ with three different lithium contents.

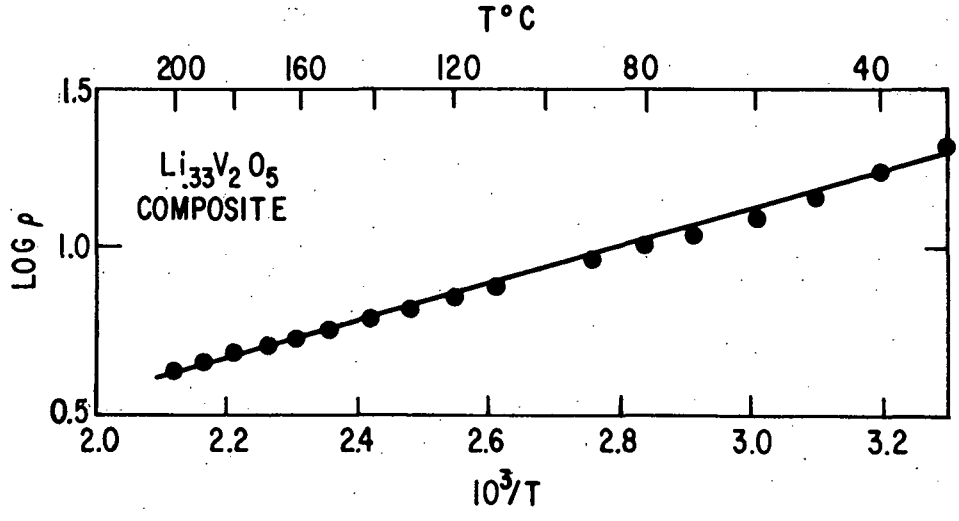

Figure 13 Log resistivity vs reciprocal temperature for a composite made by melting $Li_{0.33}V_2O_5$ into porous, sintered Al_2O_3.

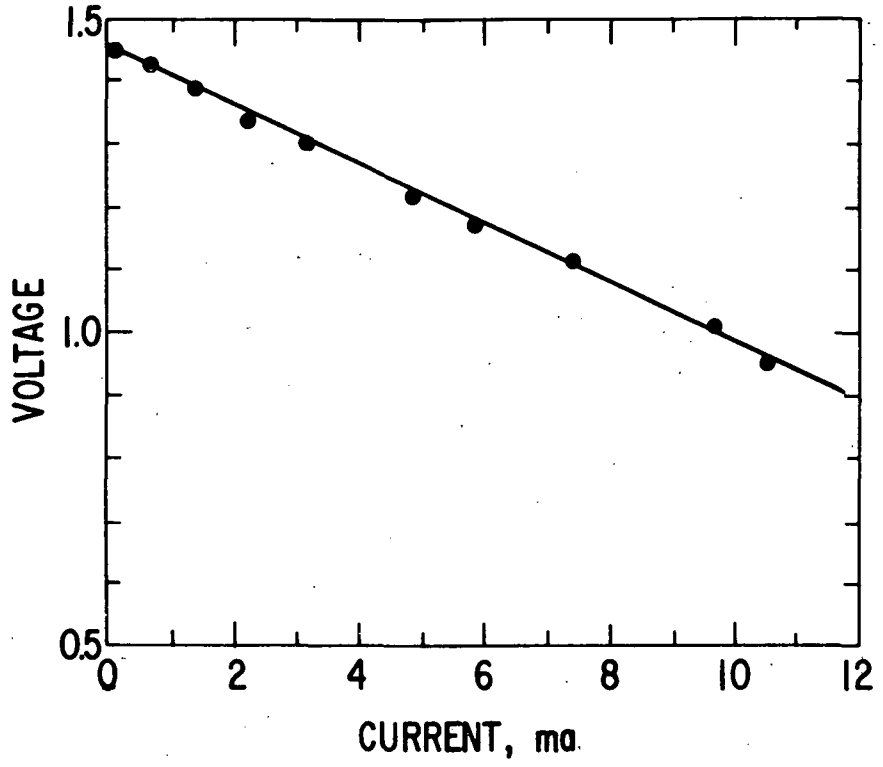

Figure 14 Voltage as a function of current of a Ni-Cd cell with a bar of $Li_{0.33}V_2O_5$ between the electrodes.

indicated a resistivity of 0.7 ohm cm, so that the sample resistance exclusive of electrode losses would be considerably less than 10^{-1} ohms. The current-voltage plot using nickel-cadmium plates and a 10% LiOH solution is shown in Fig. 14. The slope indicates a resistance of forty six ohms.

The remainder of the transport experiments were performed on sintered bars of the compositions $Li_{0.1}V_2O_5$, $Li_{0.33}V_2O_5$, and $Li_{0.6}V_2O_5$. As stated earlier the densities of the bar samples were only about 70%. In order to avoid penetration of the LiOH solution the pores were filled with a polystyrene laquer prior to making the electrical measurements. The experimental arrangement used was that shown on Fig. 3a. The results are given on Table VII with values of R_i/R_e and t_i calculated by equations 6 and 7 or 8 and 9 as appropriate. The resistivity was determined by the 4 probe a.c. method and therefore avoid contact resistances. It is noticeable that the values of total resistivity vary from sample to sample of the same composition, and also for a given sample (indicated by the letter in the sample number) made at different times. It is thought that this is due to interaction of the sample with the atmosphere. Only in experiment D3 were reference electrodes used. It can be seen than $E_0 = E_R + E$ as deduced in the introduction. The variation in E_0 is due to the state of charge of the battery plates at the time of the experiments.

TABLE VII

Data and Results of Four Terminal Transport Experiments

Experiment	Composition	E_0	E	E_R	Total Resistivity ohm cm	R_i/R_e	t_i	Ionic Resistivity ohm cm
A1	$Li_{0.1}V_2O_5$	1.120	0.001	--	175	222	0.0045	39,000
A2	$Li_{0.1}V_2O_5$	1.091	0.003	--	351	73	0.014	26,000
B1	$Li_{0.33}V_2O_5$	1.350	0.010	--	16.8	26.8	0.036	400
C2	$Li_{0.6}V_2O_5$	0.820	0.381	--	135	0.23	0.81	163
C2	$Li_{0.6}V_2O_5$	1.077	0.730	--	405	0.096	0.91	450
D1	$Li_{0.6}V_2O_5$	1.329	0.214	--	96	0.81	0.55	175
D2	$Li_{0.6}V_2O_5$	1.335	0.455	--	350	0.30	0.77	460
D3	$Li_{0.6}V_2O_5$	1.435	0.382	1.052	96	0.42	0.68	140

TABLE VIII

Values of E with Simulated Contact Resistance

Resistances	E
∞	1.077
10K	.872
1K	.742
100Ω	.713
10Ω	.715
0	.704

In order to evaluate the importance of electronic contact resistance at points V_2 and V_3, experiments were performed placing resistors in the electronic legs, that is between both working electrodes and the contact points V_2 and V_3. Table VIII gives the values of E when two identical resistors of varying magnitude were placed in each leg in experiment C2. It is apparent that contact resistancies would have to be of the order of 1000 ohms to significantly effect the results.

In all experiments where hydroxide moistened filter paper was placed between the sample and the battery plates, it was observed that the paper became discolored indicating that at least one phase of the $Li_xV_2O_5$ was dissolving. This would make it very difficult to maintain electronic contact in experiments where the plates were pressed against the samples and makes it very likely that reactions indicated here by ϵ_1 and ϵ_2 are operative.

The two probe transport measurements performed on bars and disks always resulted in values of E equal to E_0. This along with the observations of sample dissolution lead to the conclusion that in two probe measurements of this type on $Li_xV_2O_5$ the experiment is equivalent to that represented by the circuit of Fig. 2c. No conclusions can be made concerning the transport number for ions from these experiments.

The four probe experiments indicate that $Li_xV_2O_5$ is a mixed conductor. The ionic conductivity with x equal to 0.33 and 0.6 is between 10^{-2} and 10^{-3} $ohm^{-1}cm^{-1}$ and two orders of magnitude lower at $x = 0.1$. The electronic conductivity is highest at $x = 0.33$.

A simple technique has been devised to determine transport number for ions. However, it is necessary to be certain that contact resistance at the center probes is not larger than the resistance of the sample. Although we have indications that contact resistances were not significantly large a quantitative measurement has not been obtained. Until that time the ionic conductivities reported must be considered qualitative only.

$Li_xTa_2O_5$

Sample Preparation

Five compositions with x values of 0.2, 0.3, 0,4, 0.5, and 0.6 were prepared by mixing appropriate compositions of $LiNO_3$ (Reagent grade, Baker and Adamson) and Ta_2O_5 (CIBA 99.9% pure), heating to 1100°C in air for 18 hours, and ball milling. X-ray diffraction showed the products were complex mixtures of three or more phases. None of the phases were definitely identified but one appeared to be a monoclinic phase which is probably a solid solution of Li_2O in β-Ta_2O_5 and a second was probably hexagonal lithium meta tantalate.

Bars and disks were prepared by pressing at 19,000 psi. Subsequent hydrostatic pressing at 100,000 psi resulted in very fragile bars and was discontinued. Best densities were obtained by firing in air at 1550°C but the highest density specimen had at least 1% open pores. The highest density was obtained for the composition with lowest lithium content: samples with x = 0.2 averaged 3% open pores, other compositions averaged about 10% open pores.

NMR Screening

The ^7Li NMR spectra in $Li_xTa_2O_5$ show symmetric line shapes with dipolar broadening only, that is, in contrast to $Li_xV_2O_5$ there were no effects of frequency on the line width and shape. The absence of a Knight shift suggests the electronic component of the conductivity will be small.

Table IX gives the temperature dependence of the central line width of the ^7Li resonance. Strong motional narrowing at room temperature indicates there is at least short range mobility of lithium in at least one of the lithium tantalum oxide compounds in the mixture.

Figure 15 shows a Hendrickson-Bray curve from which an activation energy of 3700 cal/mole and a range parameter of 4×10^{-3} gauss is found. These values are in the range expected for localized motion but the analysis is even less certain than the previous one because of the multiphase nature of the specimen.

Motional narrowing was observed in several other specimens prepared with different compositions but detailed measurements were not made because the phases present could not be identified. In general, however,

TABLE IX

Temperature Dependence of NMR Spectrum of ^7Li in $Li_xTa_2O_5$
ν_0 = 28.0 MHz

Temperature (°C)	Peak-to-Peak Width (gauss)
-170	1.5 ± 0.1
-104	1.5 ± 0.1
- 78	1.4 ± 0.1
- 56	1.4 ± 0.1
- 32	1.25 ± 0.1
- 23	1.20 ± 0.15
RT	0.93 ± 0.05
40	0.90 ± 0.05
60	0.73 ± 0.10
80	0.58 ± 0.02
100	0.50 ± 0.02
120	0.36 ± 0.04
130	0.34 ± 0.03
163	0.27 ± 0.02
277	0.20 ± 0.02

motional narrowing of the ^7Li nucleus at relatively low temperature was observed in all of the compositions.

Conductivity

Resistivities from room temperature to 200°C of the five lithium tantalum oxide compositions are given in Fig. 16. The scatter at low temperatures is probably due to surface conduction from atmospheric water absorption. The higher temperature values indicate an activation energy between 10,000 and 20,000 cal/mole and an increase in conductivity with increasing lithium content. Little significance can be attributed to these results because of the multiphase character of the specimens.

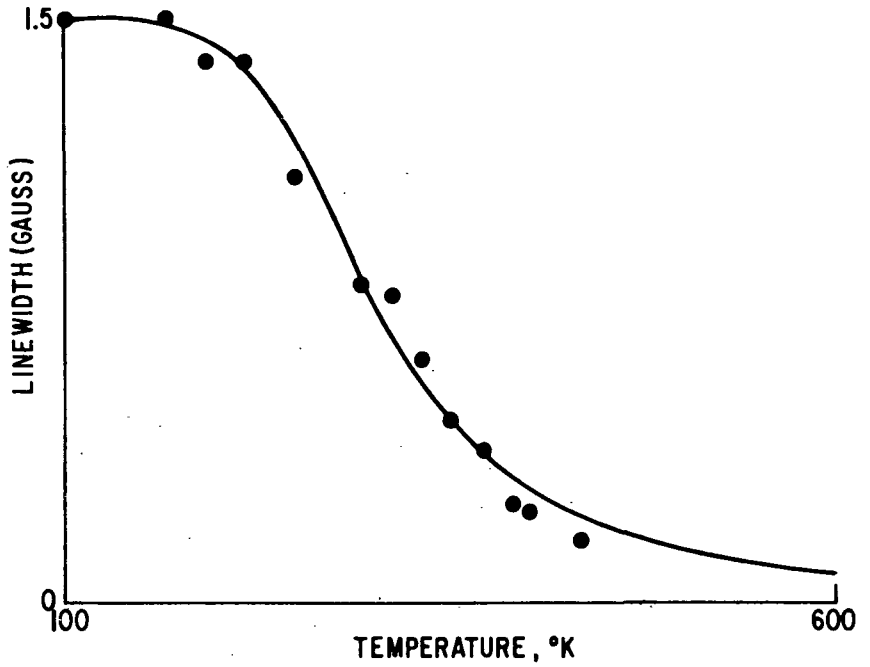

Figure 15 Temperature dependence of ^7Li NMR spectrum in $LiTa_2O_5$.

Zeolite · $LiNO_3$

Sample Preparation

Pellets of Linde molecular sieve 4A were exchanged in molten $LiNO_3$ at 350°C for two hours following the procedure outlined by Liquornik and Marcus.[28] The excess lithium nitrate was drained off and the product washed and vacuum dried four times over a period of two hours, then vacuum dried at 120°C for an additional two hours. A weight gain of 24% was determined on the specimen for NMR evaluation. A similar sample prepared the same way was found to contain 3.93 weight percent lithium by chemical analysis.

NMR Screening

The ^7Li spectrum of $LiNO_3$ occluded in zeolite shows a single symmetrical resonance peak. The temperature dependence of the line width is given in Table X. The narrowing shows motion of lithium nuclei above room temperature.

A Hendrickson-Bray plot of the temperature dependence of the line widths is given in Fig. 17. The parameters of the curve correspond to an activation energy of 9000 cal/mole and a range parameter of 3×10^{-7} gauss. These values are much like those Hendrickson and Bray find for systems in which it is believed there is long range diffusion.

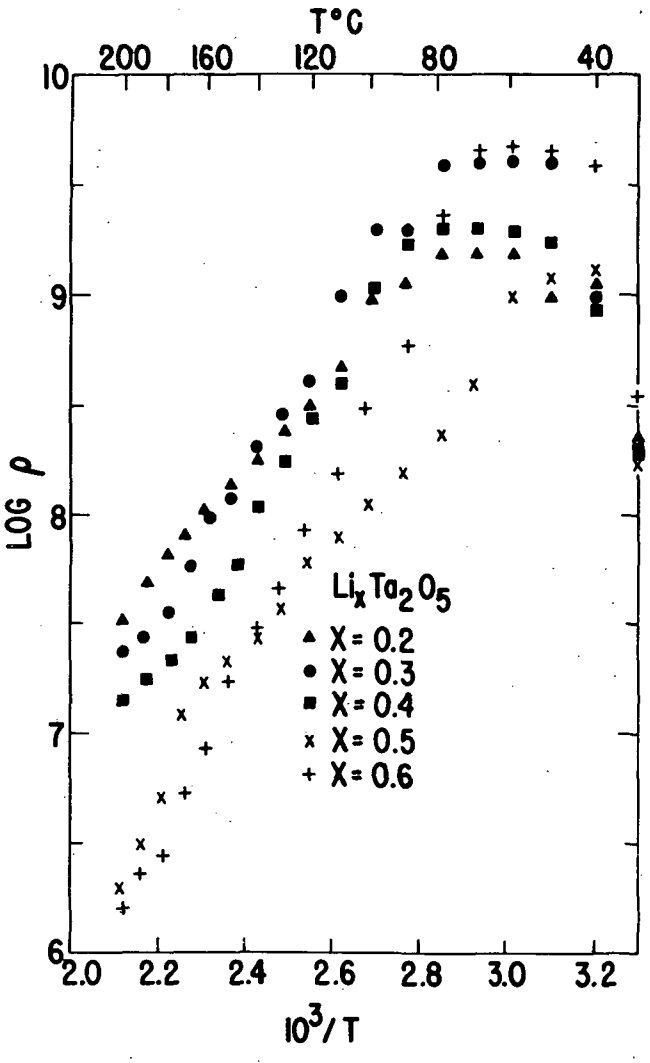

Figure 16 Log resistivity vs reciprocal temperature for different lithium contents in $Li_xTa_2O_5$.

In order to see a difference, if any, between the ^7Li NMR line in the pure compound and in the $LiNO_3$ complex, the spectrum of crystalline $LiNO_3$ was measured. The line width was 0.3 ± 0.1 gauss at room temperature and remained virtually unchanged at 0.4± 0.1 gauss when heated to 173°C showing lower temperature measurements are required to observe the rigid lattice width. The ^7Li spectra in the two states appear to be different and it is tentatively concluded there may be a change in the structure of $LiNO_3$ when it is occluded in a zeolite cavity. More work would be necessary to establish if the presence of water is required for the motional narrowing.

TABLE X

Temperature Dependence of NMR Spectrum of ^7Li in Zeolite· $LiNO_3$
ν_0 = 28,0 MHz

Temperature (°C)	Line Width (gauss)
-154	2.60 ± 0.20
- 80	2.53 ± 0.20
- 47	2.40 ± 0.20
- 18	2.20 ± 0.15
0	1.80 ± 0.15
RT	0.75 ± 0.10
38	0.75 ± 0.05
95	0.55 ± 0.02

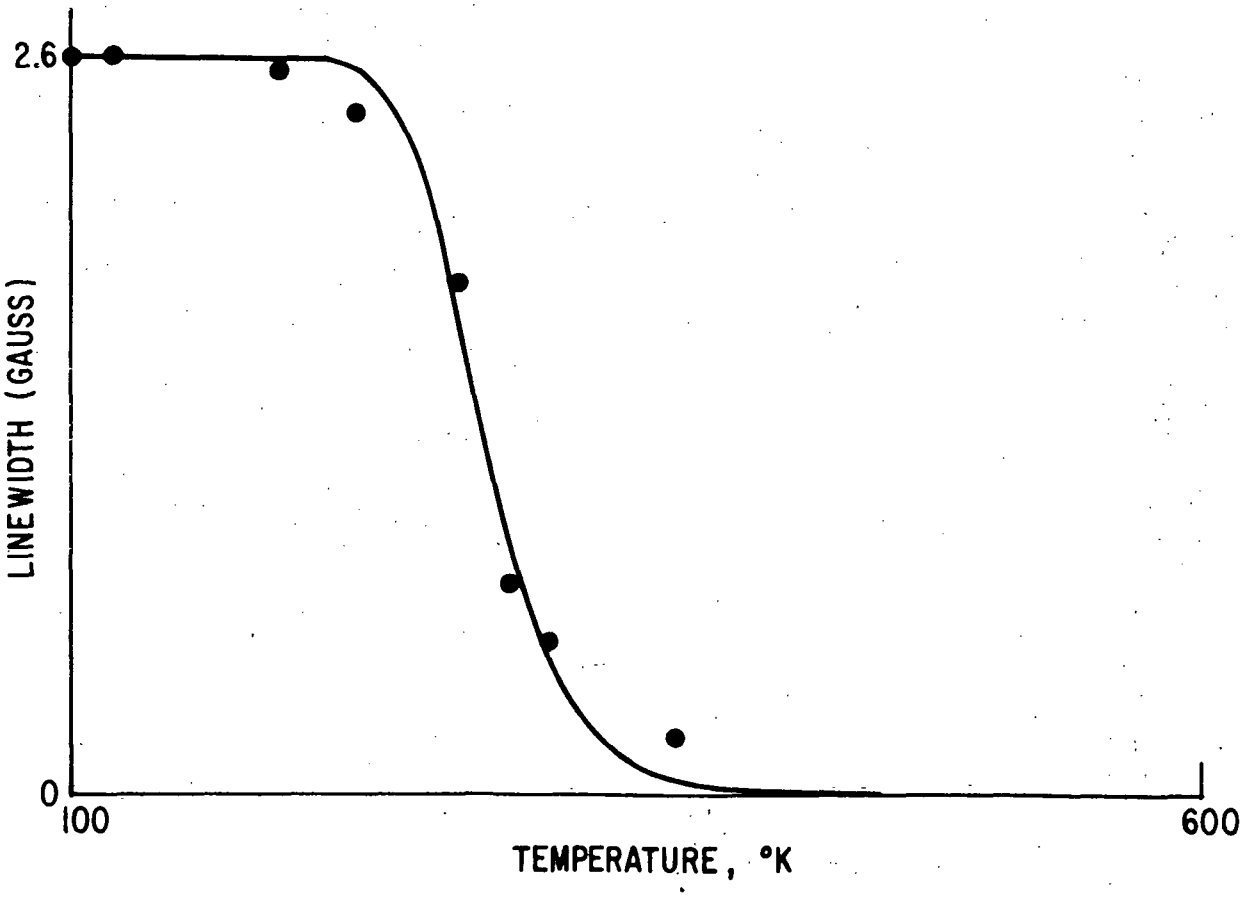

Figure 17 Temperature dependence of ^7Li NMR spectrum in $LiNO_3$ · zeolite complex.

TABLE XI

Temperature Dependence of NMR Spectrum of ^{23}Na in Na_2BeF_4
ν_0 = 19.0 MHz

Temperature (°C)	Peak-to-Peak Width (gauss)
RT	35 ± 3
60	35 ± 3
100	35 ± 3

Na_2BeF_4

Sample Preparation

Sodium beryllium tetrafluoride was purchased from Ozark Mahoning (95% pure). The powder was sealed in glass tubes for NMR analysis but because of the hazardous nature of the material conductivity bars were not fabricated. X-ray diffraction showed the material was well-crystallized, single phase orthorhombic Na_2BeF_4.

NMR Screening

Table XI gives the ^{23}Na NMR spectrum measured at room temperature, 60°C and 100°C.

The peak-to-peak separation of the ^{23}Na NMR spectrum is constant over the temperature range investigated and the absence of motional narrowing shows the sodium ions are tightly bound and will not migrate at low temperature. This does not eliminate the possibility that sodium might migrate in one of the high temperature modifications, or in a doped specimen containing defects.

$NaPrF_4$

Sample Preparation

Phase diagrams and procedures for synthesis of sodium-rare earth fluorides are given by Thoma et al.[21] The phase diagram for $NaPrF_4$ does not show any range of stoichiometry so the 1:1 composition was made. The starting compounds were ground together and heated in argon in a platinum crucible at 800°C.

The x-ray patterns of this phase were indexed on a hexagonal cell with lattice parameters a = 6.12Å, c = 9.48Å. Its structure is probably the disordered β-$NaThF_6$ arrangement.

NMR Screening

Since fluorite related structures can be either cation or anion conductors, both sodium and fluorine spectra were measured. Table XII gives the temperature dependence of the width of the ^{23}Na spectrum measured at 19.0 MHz and the ^{19}F spectrum measured at 28.0 MHz. Two fluorine peaks were observed indicating to different kinds of fluorine sites.

Motional narrowing of the sodium and one of the fluorine resonances is observed. Since both the ^{23}Na and ^{19}F spectra are motionally narrowed, either one or both nuclei may be moving.

$Na_{1+x}Yb_{1-x}F_{4-2x}$

Sample Preparation

The phase diagram shows an extended single phase fluorite solid solution region at 700°C. Therefore in the hope of producing sodium interstitials and fluorine vacancies the composition selected was $Na_{1.1}Yb_{0.9}F_{3.8}$. Sodium ytterbium fluoride was prepared by mixing sodium and ytterbium fluorides and heating at 700°C for 16 hours in argon in a platinum crucible. X-ray diffraction indicated the phase could be an orthorhombic variant of a fluorite-type cell.

TABLE XII

Temperature Dependence of ^{23}Na and ^{19}F NMR Spectra in $NaPrF_4$

Temperature (°C)	^{23}Na Peak Width (gauss) ν_0 = 28.0 MHz	Temperature (°C)	^{19}F Peak Width (gauss) Peak I	Peak II (ν_0 = 28.0 MHz)
-123	13.0 ± 2.0			
- 37	10.0 ± 2.0			
RT	9.0 ± 1.0	RT	21.0±1.0	5.0±1.0
95	8.5 ± 1.0			
173	8.5 ± 1.0	171	15.0±1.0	5.0±1.0

TABLE XIII

Temperature Dependence of ^{23}Na and ^{19}F NMR Spectra in $11NaF \cdot 9YbF_3$

Temperature (°C)	^{23}Na Line Width (gauss) ν_0 = 19.0 MHz	Temperature (°C)	^{19}F Line Width (gauss) ν_0 = 28.0 MHz
-123	27.0 ± 5.0		
- 37	19.0 ± 3.0		
RT	17.0 ± 1.0	RT	21.0 ± 1.0
95	13.0 ± 2.0	140	12.0 ± 1.0
173	12.0 ± 2.0	171	10.0 ± 2.0

NMR Screening

Since fluorites may be either cation or anion conductors the spectra of the ^{23}Na and ^{19}F nuclei were both measured. The line widths as a function of temperature are given in Table XIII. As in the hexagonal $NaPrF_4$ phase, both sodium and fluorine spectra show motional narrowing and either, or both, may be moving.

$NaTa_5TiO_{15}$

Sample Preparation

This material was prepared from reagent grade $NaNO_3$, TiO_2, and purified Ta_2O_5 by reaction for 16 hours in a platinum crucible in air at 1000°C. The resulting powder was ground to -325 mesh. A bar for conductivity measurements was pressed at 2,000 psi and fired at 1000°C. The density of the conductivity bar was less than 70%.

The diffraction pattern of the product could not be identified and did not correspond to any of the sodium tantalum oxide patterns in the x-ray files.

NMR Screening

The formula $NaTa_5TiO_{15}$ was conceived as a charge compensated analog of $LiTa_3O_8$ with sodium ions lying in tunnels. The synthetic product was screened for sodium mobility by measurement of the ^{23}Na NMR spectrum at ν_0 = 19.0 MHz. The peak-to-peak separation at room temperature was about 9 gauss. At 264°C the overall line width narrowed to 6 gauss suggesting there is motion of the sodium at the elevated temperature. The shape of the spectrum was different at high and low temperature but because of the weak signal intensity a more systematic study could not be made in the time period.

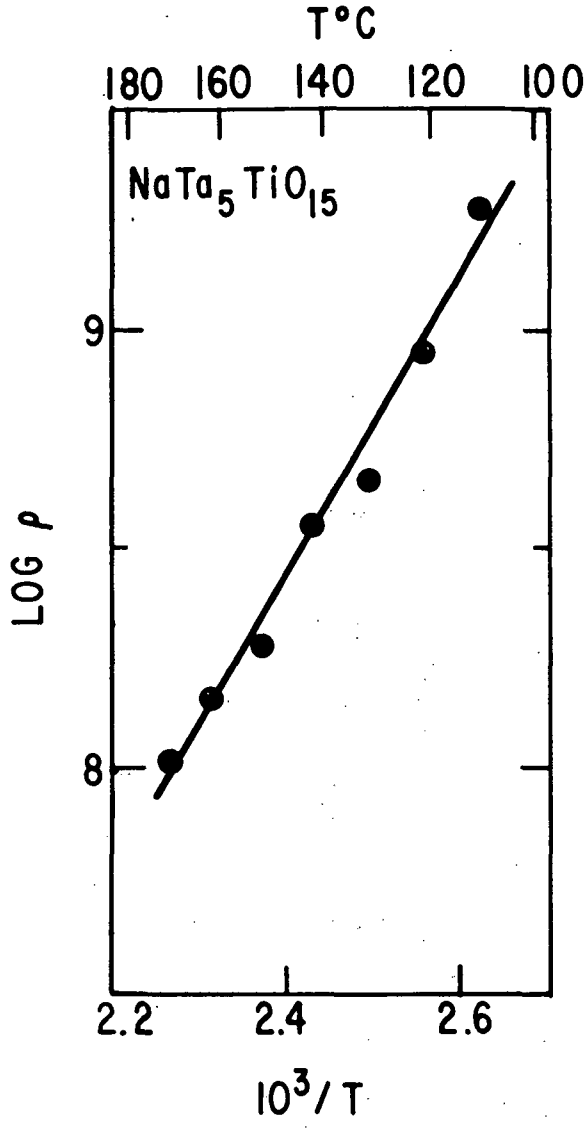

Figure 18 Log resistivity vs reciprocal temperature for $NaTa_5TiO_{15}$.

Conductivity

The resistivity-temperature behavior of a 70% dense conductivity bar is given on Fig. 18. The conductivity is low and the activation energy is 16,000 cal/mole. Little effort was given to sample densification and the low conductivity associated with small activation energy indicate the data are not representative of intrinsic bulk behavior.

$NaCaPO_4$

Sample Preparation

Sodium calcium phosphate was synthesized by grinding and mixing reagent grade Na_3PO_4 with purified (Fischer) $Ca_3(PO_4)_2$ and firing for 16 hours at 1100°C as suggested by Klement and Kresse.[17] X-ray diffraction showed the product was multiphase and apparently consisted of a mixture of at least three low and high temperature forms. Bar shaped samples were obtained by pressing at 5300 lbs and firing in air at 900°C.

NMR Screening

The ^{23}Na NMR resonance in the multiphase $NaCaPO_4$ mixture was measured at six different temperatures to see if there was an indication of motional narrowing in any of the forms. The ^{23}Na peak-to-peak separation was 11.0 ± 1.0 gauss at room temperature. Within experimental error the overall width of the composite peak remained unchanged from -166°C to +231°C. However, the relative intensities of the peaks varied as a function of temperature. At lower temperature the intensity of the high frequency side peak was stronger than that of the low frequency side peak, and at higher temperature the relative intensity ratio of the two was reversed.

The dependence of peak shape on temperature may be evidence for motion of the sodium nuclei in one or more of the phases, or to phase transformations which change the crystal field environments of the sodium nuclei. Further investigations with single phase materials would be required to settle this question.

Conductivity

Figure 19 gives the results of four probe a.c. resistivity data obtained on a bar sample of $NaCaPO_4$. The conductivity bar was highly porous and the resistivity was so high that measurements could be made only at temperatures greater than 500°C. The overall activation energy was 18,000 cal/mole but the significance of this value is questionable in view of the multiphase and porous nature of the test specimen.

$NaBO_2$

Sample Preparation

Sodium metaborate was prepared by the method given by Fang.[19] Reagent grade Na_2CO_3 and purified (J.T. Baker) B_2O_3 were ground together and heated for 2 hours in a platinum crucible in air at 1000°C, reground and heated 2 hours at 700°C, reground and heated two hours at 1000°C, and finally reground and heated again for 2 hours at 700°C. The absence of a reaction

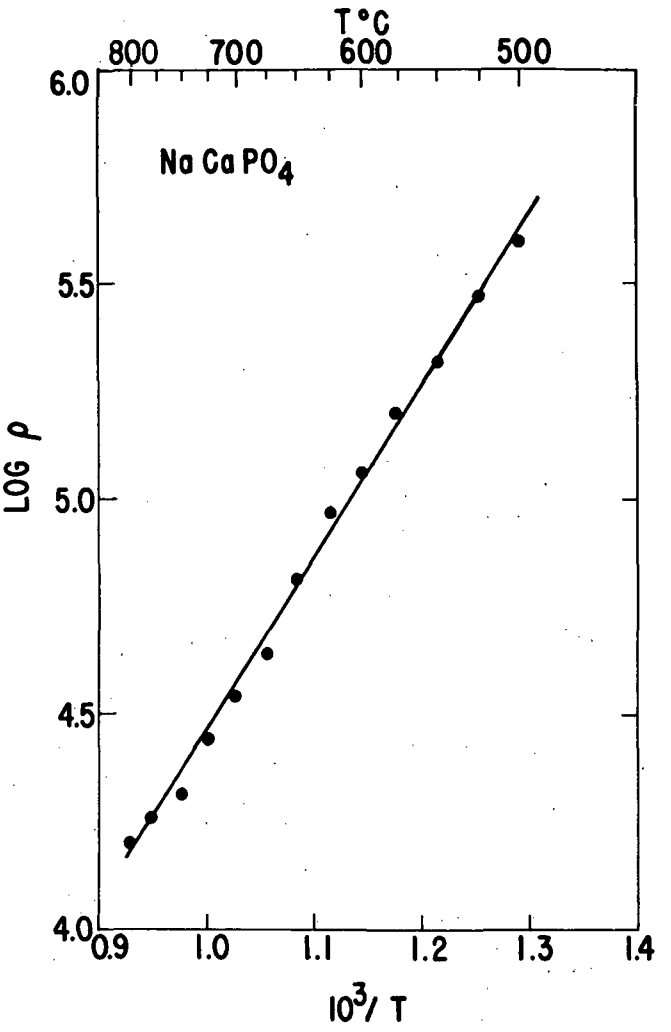

Figure 19 Log resistivity vs reciprocal temperature for $NaCaPO_4$.

with HNO_3 indicated complete CO_2 loss. Material that was purchased as $NaBO_2$ (Mathewson, Colman, and Bell) and dried at 200°C was found to be $Na_2B_2O_4 \cdot H_2O$.

Conductivity bars were prepared from the commercial material in the usual manner by firing at 750°C.

NMR Screening

Sodium metaborate was screened to determine whether the interstices between the large, planar $B_3O_6^{-2}$ ions were sufficiently open to permit sodium ion migration. The first spectrum that was obtained proved to be from the hydrate, $Na_2B_2O_4 \cdot H_2O$. The line width of the ^{23}Na NMR spectrum was only 1.0 ± 0.2 gauss at room temperature, suggesting motion of the sodium nuclei.

The phase was not evaluated further because hydrated salts would not be stable in the reactive chemical environments required for high energy density applications.

The peak-to-peak width of the ^{23}Na spectrum in anhydrous $NaBO_2$ was 7.0 ± 0.5 gauss, indicating negligible motion of sodium at room temperature. Although this conclusion cannot be considered firm in the absence of spectra at higher temperature, the prospects were considered poor and work on this compound was discontinued.

Conductivity

The pressed and fired bars were well sintered and contained only 1% open pore volume. The conductivity was very low, 10^{-8} ohm^{-1} at 200°C and less than $10^{-10} ohm^{-1} cm^{-1}$ at room temperature, showing that undoped polycrystalline $NaBO_2$ is a very poor conductor up to 200°C.

K_2TiF_6

Sample Preparation

Potassium titanium hexafluoride purchased from Pfaltz and Bauer was fabricated into bars for conductivity measurements. Specimens were not prepared for NMR screening because the potassium spectrum is weak and difficult to observe. Hot pressed samples were made as 1" disks by pressing in graphite dies at 2000 psi and 550°C. They were 93% of theoretical density, and x-ray analysis showed the product was single phase trigonal K_2TiF_6. Bars that were hydrostatically repressed at 200,000 psi and direct at 700°C were only 40% dense and shown by x-ray diffraction no longer to be trigonal K_2TiF_6.

Conductivity

Preliminary tests on K_2TiF_6 resulted in rather encouraging resistivity results, i.e., 2×10^4 ohm cm at 200°C. Considering the low density of the first samples attempts were made to improve the conductivity by increased densification. The conductivities of hot pressed samples are shown on Fig. 20. Refiring of the hot pressed sample resulted in the increased conductivity also shown on Fig. 20. As noted above, the hot pressed material was trigonal K_2TiF_6 and sintering at one atmosphere pressure resulted in a product of unknown structure, or mixture of structures, with higher conductivity. Considering the complexity of the results and the absence of NMR data, continuation of work on this system was terminated.

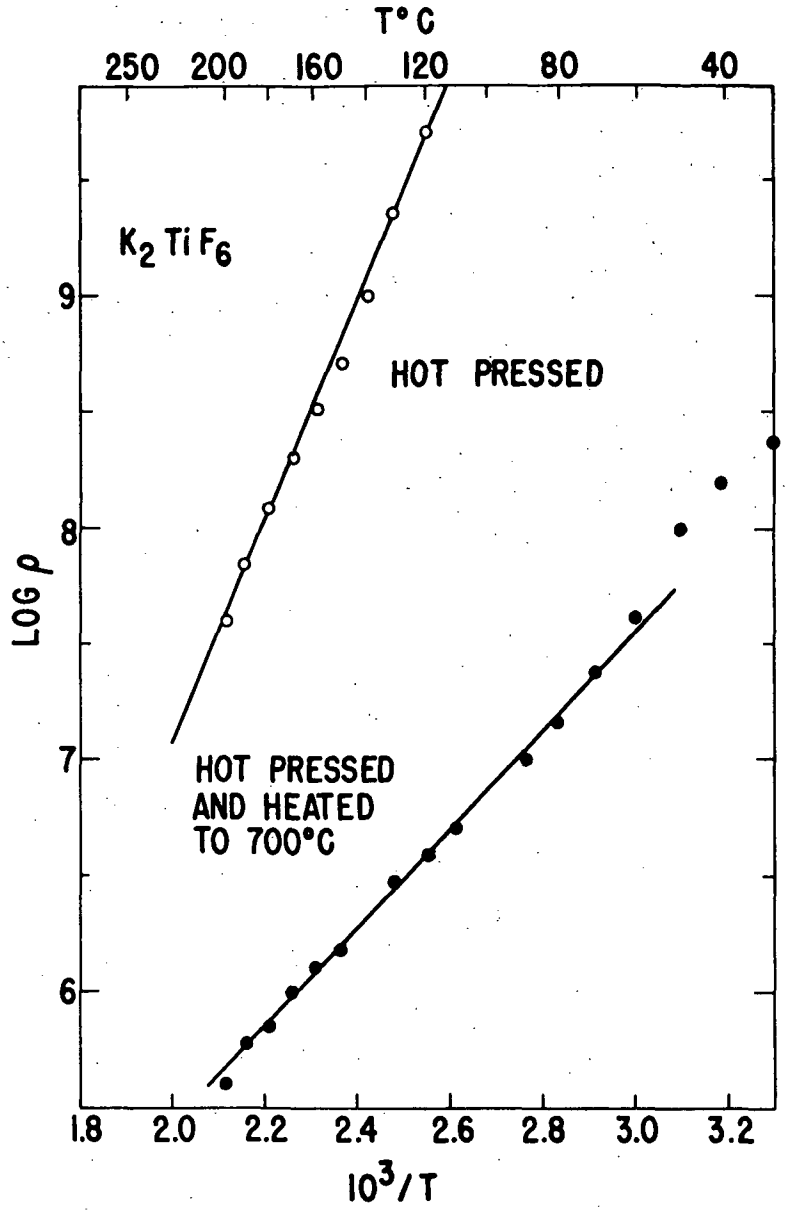

Figure 20 Log resistivity vs reciprocal temperature for hot pressed K_2TiF_6. Reheating decreases resistivity.

Framework Minerals

Many alumina-silicate minerals have open framework structures with a variety of cations in the interstices. These compositions and structures tend to be extremely complicated and a few natural specimens were screened for evidence of ion motion. In nearly every case the composition and purity of the mineral proved to be questionable. The names of the minerals and the

nuclei whose spectra were measured are as follows:

Mineral	Nucleus
Ultramarine Blue	Na
Hackmanite	Na
Eucryptite	Li
Pollucite	Na
Sodalite	Na
Nepheline	Na

Motional narrowing was not observed in any of the mineral specimens but definitive conclusions cannot be drawn because the spectra were exceedingly weak and the desired compound may have been present in small concentration.

IV. CONCLUSIONS

A wide variety of structure types and materials with differing degrees of purity were screened for evidence of ion motion at low temperature. A summary is given in Table XIV of the successes and failures that were had in utilizing crystal structure principles to predict structures and specific compounds through which ions could easily migrate. The criterion for ion motions is the observation of significant motional narrowing of the NMR spectrum in the vicinity of room temperature.

A general observation that can be made is that successful predictions were made for compounds that crystallized in tunnel structures, fluorite-related structures, and nonstoichiometric disordered structures. On the other hand, there was no evidence for ion motion in compounds with large open interstices when the compounds had crystallized in well-ordered arrangements. It is possible these latter compounds would develop ionic mobility if they were heat treated or doped to develop nonstoichiometry. However, the results give little encouragement to the idea that NMR can be used to detect a "loosening" of the structure, or large anticipatory vibrations, which can be used to predict which arrangements may be reasonable candidate for synthesis in a nonstoichiometric state.

Several important conclusions were reached as a result of the search for new solid electrolytes which will lead to a refinement of the structural criteria that will be applied in the future. Nonstoichiometric compounds frequently contain ions in more than one valence state. Typical examples are the lithium vanadates. Multiple valence state usually result in considerable electronic conduction which makes it difficult to assess the amount of charge transported by ions. The electronic conduction may be reduced if charge compensating ions can be incorporated without destroying the desired structure. Several open framework or low density compounds were relatively stoichiometric and contained only a small concentration of defects. Such solids were tested with the hope that they would exhibit some motional narrowing of the NMR spectrum, thus indicating ionic motion, and that the level of mobility could be enhanced by additives to create more defects. Examples for such compounds are $NaBO_2$ and Na_2BeF_4. However, none of these compounds gave evidence for potential ion motion and screening in the future should be limited to compounds which are known to contain defects.

The measurement of motional narrowing of the NMR spectrum has proven to be an excellent and efficient method to screen powders of candidate materials for potential ionic conductivity. It should be emphasized that motional narrowing with increasing temperature is a necessary but not sufficient condition for ion transport. Nevertheless, the possibility of arriving at a first rapid evaluation of relatively impure powder specimens has been of great value in permitting the screening of a much larger number of candidate materials than

TABLE XIV

Summary of NMR Screening Tests

Compound	Mobile Ion	Structure	Motional Narrowing Yes	Doubtful	No
Li_3AlN_2	Li	Antifluorite	X		
Li_3BN_2	Li	Antifluorite	X		
$LiAl_5O_8$	Li	Spinel			X
$Li_{0.3}V_2O_5$	Li	Tunnel	X		
$LiTa_2O_5$	Li	Tunnel	X		
$NaCaPO_4$	Na	Open		X	
Na_2BeF_4	Na	Open			X
$NaTa_5TiO_{15}$	Na	Tunnel	X		
$LiNb_{16}O_{15}F$	Li	Tunnel	X		
$LiNO_3$ · zeolite	Li	Interconnect cavities	X		
$NaPrF_4$	Na	Disordered β-$NaThF_6$	X		
$NaPrF_4$	F	Disordered β-$NaThF_6$	X		
$NaYbF_4$	Na	Fluorite	X		
$NaYbF_4$	F	Fluorite	X		
$NaBO_2$	Na	Open			X
Ultramarine	Na	Framework		X	
Hackmanite	Na	Framework		X	
Eucryptite	Li	Framework		X	
Pollucite	Na	Framework		X	
Sodalite	Na	Framework		X	
Nepheline	Na	Framework		X	

possible otherwise. There is also a possibility that a detailed analysis of the spectra may allow a distinction between short or long range motion.

Several limitations of NMR screening became clear during the work to date which suggest the following modifications of the method for future work.

(1) The potassium spectrum is too weak to be measured in a reasonable amount of time with the present equipment. For practical purposes, screening should be limited to materials in which the charge is carried by lithium, sodium, hydrogen, or fluoride ions.

(2) Excessive quantities of impurities, that is, more than 10% to 20%, make evaluation less certain. This is particularly true if the impurity contains atoms of the same kind as the charge carrier in the ionic conductor since the spectra may overlap and mask line narrowing in the phase of interest. Consequently, some more emphasis on purification is essential.

V. REFERENCES

1. Reuter, B. and Hardell, K., Naturwissenschaften, 48, 161 (1961).
2. Yao, Y.F. and Kummer, J.T., J. Inorgan. Nucl. Chem., 29, 2453 (1967).
3. Carter, R.E. and Roth, W.L., Electomotive Force Measurements in High Temperature Systems, pp 125-148; The Institute of Mining and Metallurgy, Grosvenor Press, Portsmouth, England (1968).
4. Rice, M.J. and Roth, W.L., J. of Solid State Chem., 4, 294 (1972).
5. Juza, R. and Hund, F., Z. für anorg. Chemie, 257, 13 (1948).
6. Goubeau, J. and Anselment, W., Z. für anorg. und allgem. Chemie, 310, 248 (1961).
7. Kordes, E., Z. Krist., 91, 193 (1935).
8. Verwey, E.J.W. and Heilman, E.L., J. Chem. Phys., 15, 174 (1947).
9. Datta, R.K. and Roy, R., J. Am. Cer. Soc., 46, 388 (1963).
10. Bettman, M. and Peters, C.R., J. Phys. Chem., 73, 1774 (1969).
11. Lundberg, M., Acta Chem. Scand., 19, 2274 (1965).
12. Hardy, A., Galy, J., Casalot, A., and Bouchard, M., Bull. Soc. Chim. France, 6, 1056 (1965).
13. Galy, J., Darriet, J., Casalot, A., and Goodenough, J.B., J. Solid State Chem., 1, 339 (1970).
14. Reisman, A. and Haltzberg, F., J. Amer. Chem. Soc., 80, 6503 (1958).
15. Whiston, C.D. and Smith, A.J., Acta Cryst., 19, 169 (1965).
16. Jahnberg, L., J. Solid State Chem., 1, 454 (1970).

17. Klement, R. and Kresse, P., Z. für anorg. und allgem. Chemie, 310,

18. Wykoff, R. W. G., Crystal Structures, Vol. 3.

19. Fang, S., Z. für Krist., 99, 1 (1938).

20. Burns, J. H., Inorg. Chem., 4, 881 (1965).

21. Thoma, R. E., Insley, H., and Herbert, G. M., Inorganic Chemistry, 5, 1222 (1966).

22. Roy, D. M. and Roy, R., J. Electrochem. Soc., 111, 421 (1964).

23. DeVries, R. C. and Fleischer, J. F., Mat. Res. Bull, 4, 433 (1969).

24. Bishop, S. G., Ring, P. J., and Bray, P. J., J. Chem. Phys., 45, 1525 (1966).

25. Kessler, H. and Sienko, M. J., J. Solid State Chem., 1, 152 (1970).

26. Hagenmuller, P., Galy, J., Pouchard, M., and Casalot, A., Mat. Res. Bull., 1, 45 (1966).

27. Gendell, J., Cotts, R. M., and Sienko, M. J., J. Chem. Phys., 37, 220 (1962).

28. Liquornik, M. and Marcus, Y., J. Phys. Chem., 72, 2885 (1968).

Contract NAS3-15692

DISTRIBUTION LIST

NASA

National Aeronautics and Space Administration
Scientific and Technical Information Facility
P.O. Box 33
College Park, MD 20740
(2 copies and 1 reproducible)

Mr. Ernst M. Cohn, Code RPP
National Aeronautics and Space Administration
Washington, DC 20546

Dr. A.M. Greg Andrus, Code SCC
National Aeronautics and Space Administration
Washington, DC 20546

Mr. Gerald Halpert, Code 764
Goddard Space Flight Center
National Aeronautics and Space Administration
Greenbelt, MD 20771

Mr. Thomas Hennigan, Code 761
Goddard Space Flight Center
National Aeronautics and Space Administration
Greenbelt, MD 20771

Mr. Louis Wilson, Code 450
Goddard Space Flight Center
National Aeronautics and Space Administration
Greenbelt, MD 20771

Mr. Albert Antoine (35 cc)
Lewis Research Center
National Aeronautics and Space Administration
21000 Brookpark Road
Cleveland, OH 44135

Mr. Jack E. Zanks, MS 488
Langley Research Center
National Aeronautics and Space Administration
Hampton, VA 23365

Dr. Louis Rosenblum, MS 302-1
Lewis Research Center
National Aeronautics and Space Administration
21000 Brookpark Road
Cleveland, OH 44135

Mr. Harvey Schwartz, MS 309-1
Lewis Research Center
National Aeronautics and Space Administration
21000 Brookpark Road
Cleveland, OH 44135

Dr. J. Stuart Fordyce, MS 309-1
Lewis Research Center
National Aeronautics and Space Administration
21000 Brookpark Road
Cleveland, OH 44135

Mr. Charles B. Graff, S&E-ASTR-EP
George C. Marshall Space Flt. Center
National Aeronautics and Space Administration
Huntsville, AL 35812

Mr. W.E. Rice, EP5
Manned Spacecraft Center
National Aeronautics and Space Administration
Houston, TX 77058

JPL

Mr. Daniel Runkle, MS 198-220
Jet Propulsion Laboratory
4800 Oak Grove Drive
Pasadena, CA 91103

Mr. Aiji A. Uchiyama, MS 198-220
Jet Propulsion Laboratory
4800 Oak Grove Drive
Pasadena, CA 91103

Dr. R. Lutwack, MS 198-220
Jet Propulsion Laboratory
4800 Oak Grove Drive
Pasadena, CA 91103

ARMY

U.S. Army
Electro Technology Laboratory
Energy Conversion Research Div.
MERDC
Fort Belvoir, VA 22060

Harry Diamond Laboratories
Room 300, Building 92
Connecticut Ave. & Van Ness St., N.W.
Washington, DC 20438

U.S. Army Electronics Command
Attn: AMSEL-TL-P
Fort Monmouth, NJ 07703

NAVY

Director, Power Program, Code 473
Office of Naval Research
Arlington, VA 22217

Mr. Harry W. Fox, Code 472
Office of Naval Research
Arlington, VA 22217

Mr. S. Schuldiner, Code 6160
Naval Research Laboratory
4555 Overlook Avenue, S.W.
Washington, DC 20360

Mr. J.H. Harrison, Code A731
Naval Ship R&D Laboratory
Annapolis, MD 21402

Commanding Officer
Naval Ammunition Depot
(305, Mr. D.G. Miley)
Crane, Indiana 47522

Chemical Laboratory, Code 134.1
Mare Island Naval Shipyard
Vallejo, CA 94592

Mr. Phillip B. Cole, Code 232
Naval Ordnance Laboratory
Silver Spring, MD 20910

Mr. Albert Himy, 6157D
Naval Ship Engineering Center
Center Bldg., Prince Georges Center
Hyattsville, MD 20782

Mr. Robert E. Trumbule, STIC
4301 Suitland Road
Suitland, MD 20390

Mr. Bernard B. Rosenbaum, Code 03422
Naval Ship Systems Command
Washington, DC 20360

AIR FORCE

Mr. R.L. Kerr, POE-1
AF Aero Propulsion Laboratory
Wright-Patterson AFB, OH 45433

Mr. Edward Raskind, LCC, Wing F
AF Cambridge Research Lab.
L.G. Hanscom Field
Bedford, MA 01731

Mr. Frank J. Mollura, TSGD
Rome Air Development Center
Griffiss AFB, NY 13440

HQ SAMSO (SMTAE/Lt. R. Ballard)
Los Angeles Air Force Station
Los Angeles, CA 90045

OTHER GOVERNMENT ORGANIZATIONS

Dr. Jesse C. Denton
National Science Foundation
1800 G Street, N.W.
Washington, DC 20550

PRIVATE ORGANIZATIONS

Aerospace Corporation
Attn: Library Acquisition Group
P.O. Box 95085
Los Angeles, CA 90045

Dr. R.T. Foley
Chemistry Department
American University
Massachusetts & Nebraska Aves., N.W.
Washington, DC 20016

Dr. H.L. Recht
Atomics International Division
North American Aviation, Inc.
P.O. Box 309
Canoga Park, CA 91304

Mr. R.F. Fogle, GF 18
Autonetics Division, NAR
P.O. Box 4181
Anaheim, CA 92803

Dr. John McCallum
Battelle Memorial Institute
505 King Avenue
Columbus, OH 43201

Mr. W.W. Hough
Bellcomm, Inc.
955 L'Enfant Plaza, S.W.
Washington, DC 20024

Mr. D.O. Feder
Bell Telephone Laboratories, Inc.
Murray Hill, NJ 07974

Dr. Carl Berger
13401 Kootenay Drive
Santa Ana, CA 92705

Mr. Sidney Gross
M.S. 84-79
The Boeing Company
P.O. Box 3999
Seattle, WA 98124

Mr. M.E. Wilke, Chief Engineer
Burgess Division
Gould, Inc.
Freeport, IL 61032

Dr. Eugene Willihnganz
C & D Batteries
Division of ELTRA Corporation
3043 Walton Road
Plymouth Meeting, PA 19462

Professor T.P. Dirkse
Calvin College
3175 Burton Street, S.E.
Grand Rapids, MI 49506

Mr. F. Tepper
Catalyst Research Corporation
6101 Falls Road
Baltimore, MD 21209

Mr. C. E. Thomas
Chrysler Corporation
Space Division
P. O. Box 29200
New Orleans, LA 70129

Dr. L. J. Minnich
G. & W. H. Corson, Inc.
Plymouth Meeting, PA 19462

Mr. J. A. Keralla
Delco Remy Division
General Motors Corporation
2401 Columbus Avenue
Anderson, IN 46011

Mr. J. M. Williams
Experimental Station, Bldg. 304
Engineering Materials Laboratory
E. I. du Pont de Nemours & Company
Wilmington, Delaware 19898

Dr. A. Salkind
ESB, Inc. Research Center
19 West College Avenue
Yardley, PA 19067

Mr. E. P. Broglio
Eagle-Picher Industries, Inc.
P. O. Box 47, Couples Dept.
Joplin, MO 64801

Mr. V. L. Best
Elpower Corporation
2117 South Anne Street
Santa Ana, CA 92704

Dr. W. P. Cadogan
Emhart Corporation
Box 1620
Hartford, CT 06102

Dr. G. Goodman
Globe-Union, Inc.
P. O. Box 591
Milwaukee, WI 53201

Dr. H. G. Oswin
Energetics Science, Inc.
4461 Bronx Blvd.
New York, NY 10470

Mr. Martin Klein
Energy Research Corporation
15 Durant Avenue
Bethel, CT 06801

Dr. Arthur Fleischer
466 South Center Street
Orange, NJ 07050

Dr. R. P. Hamlen
Research and Development Center
General Electric Company
P. O. Box 43, Bldg. 37
Schenectady, N. Y. 12301

Mr. Kenneth Hanson
General Electric Company
Valley Forge Space Technology Center
P. O. Box 8555
Philadelphia, PA 19101

Mr. Aaron Kirpich
Space Systems, Room M2614
General Electric Company
P. O. Box 8555
Philadelphia, PA 19101

Mr. P. R. Voyentzie
Battery Products Section
General Electric Company
P. O. Box 114
Gainsville, FL 32601

Mr. David F. Schmidt
General Electric Company
777 14th Street, N. W.
Washington, DC 20005

Dr. Richard E. Evans
Applied Physics Laboratory
Johns Hopkins University
8621 Georgia Avenue
Silver Spring, MD 20910

Dr. J. E. Oxley
Gould Ionics, Inc.
P.O. Box 3140
St. Paul, Minnesota 55165

Grumman Aerospace Corporation
S.J. Gaston, Plant 35, Dept. 567
Bethpage, Long Island
New York 11714

Battery and Power Sources Division
Gulton Industries
212 Durham Avenue
Metuchen, NJ 08840

Dr. P.L. Howard
Centreville, MD 21617

Dr. M.E. Ellion, Manager
Propulsion & Power Systems Lab.
Building 366, MS 524
Hughes Aircraft Company
El Segundo, CA 90245

Mr. R. Hamilton
Institute for Defense Analyses
400 Army-Navy Drive
Arlington, VA 22202

Dr. R. Briceland
Institute for Defense Analyses
400 Army-Navy Drive
Arlington, VA 22202

Mr. N.A. Matthews
International Nickel Company
1000-16th Street, N.W.
Washington, DC 20036

Messrs. William B. Collins and
M.S. Imamura
Martin-Marietta Corporation
P.O. Box 179, Denver, CO 80201

Mr. A.D. Tonelli, MS 17, Bldg. 22
A3-830
McDonnell Douglas Astronautics Co.
5301 Bolsa Avenue
Huntington Beach, CA 92647

Dr. A. Moos
Leesona Moos Laboratories
Lake Success Park, Community Drive
Great Neck, NY 11021

Dr. R.A. Wynveen, President
Life Systems, Inc.
23715 Mercantile Road
Cleveland, OH 44122

Dr. James D. Birkett
Arthur D. Little, Inc.
Acorn Park
Cambridge, MA 02140

Mr. Robert E. Corbett
Department 62-25, Building 151
Lockheed Aircraft Corporation
P.O. Box 504
Sunnyvale, CA 94088

Mr. S.J. Angelovich
Chief Engineer
Mallory Battery Company
South Broadway
Tarrytown, NY 10591

Dr. Per Bro
P.R. Mallory & Company, Inc.
Library
Northwest Industrial Park
Burlington, MA 01801

P.R. Mallory & Company, Inc.
Library
P.O. Box 1115
Indianapolis, IN 46206

Mr. Joseph M. Sherfey
5261 Nautilus Drive
Cape Coral. FL 33904

Dr. W.R. Scott (M 2/2154)
TRW Systems, Inc.
One Space Park
Redondo Beach, CA 90278

Dr. Robert C. Shair
Motorola, Inc.
8000 W. Sunrise Blvd.
Ft. Lauderdale, FL 33313

Rocketdyne Divisions
North American Rockwell Corp.
Attn: Library
6633 Canoga Avenue
Canoga Park, CA 91304

Mr. D. C. Briggs
WDL Division
Philco-Ford Corporation
3939 Fabian Way
Palo Alto, CA 94303

Power Information Center
University City Science Institute
3401 Market Street, Room 2210
Philadelphia, PA 19014

RAI Research Corporation
225 Marcus Blvd.
Hauppauge, L.I., NY 11787

Southwest Research Institute
Attn: Library
P.O. Drawer 28510
San Antonio, TX 78228

Yardney Electric Corporation
Power Sources Division
3850 Olive Street
Denver, CO 80207

Yardney Electric Division
82 Mechanic Street
Pawcatuck, CT 02891

Dr. Charles Levine
Dow Chemical U.S.A.
Walnut Creek Research Center
2800 Mitchell Drive
Walnut Creek, CA 94598

Dr. Herbert P. Silverman (R-1/2094)
TRW Systems, Inc.
One Space Park
Redondo Beach, CA 90278

TRW, Inc.
Attn: Librarian TIM 3417
23555 Euclid Avenue
Cleveland, OH 44117

Dr. Jose Giner
Tyco Laboratories, Inc.
Bear Hill
Hickory Drive
Waltham, MA 02154

Union Carbide Corporation
Development Laboratory Library
P.O. Box 6056
Cleveland, OH 44101

Dr. Robert Powers
Consumer Products Division
Union Carbide Corporation
P.O. Box 6116
Cleveland, OH 44101

Dr. C. C. Hein, Contract Admin.
Research and Development Center
Westinghouse Electric Corporation
Churchill Borough
Pittsburgh, PA 15235

Dr. Paul Jorgensen
Stanford Research Institute
Menlo Park, CA 94025

Dr. L. Topper
Div. of Advanced Technology Applications
National Science Foundation
Washington, DC 20550

Mr. L.R. Rothrock
Union Carbide Corp.
8888 Balboa Ave.
San Diego, CA 92123

Prof. Donald M. Smyth
Materials Research Center
Lehigh University
Bethlehem, PA 18015

Prof. John W. Patterson
Dept. of Metallurgy
Iowa State University
Ames, Iowa 50010

Prof. Rustum Roy
Materials Science Dept.
Pennsylvania State University
University Park, PA

Prof. John H. Kennedy
Univ. of Calif. at Santa Barbara
Santa Barbara, CA 93106

Dr. Douglas O. Raleigh
North American Rockwell Science Center
Thousand Oaks, CA 91360

Dr. Robert S. Roth
National Bureau of Standards
U. S. Department of Commerce
Washington, D. C. 20234

Prof. Harold S. Story
Dept. of Physics
State University of New York at Albany
Albany, N. Y. 12203

Dr. Robert A. Huggins
Dept. of Materials Science and Engg.
Stanford University
Stanford, CA 94305

Dr. M. Stanley Whittingham
Esso Research and Engineering Co.
Linden, New Jersey

Dr. Neill T. Weber
Ford Motor Co. Research Lab.
Dearborn, Michigan

Prof. James I. Mueller
Ceramic Engineering Div.
University of Washington
Seattle, WA 98195

Dr. R. H. Doremus
Rensselaer Polytechnic Institute
Material Division
Troy, New York 12181

Prof. Alexander F. Wells
Dept. of Chemistry
University of Connecticut
Storrs, CT 06268